SAN DIEGO STATE UNIVERSITY AND

UNIVERSITY OF CALIFORNIA

Santa Barbara

Spatial and temporal variation in biomass accumulation in southern California chaparral

A Dissertation submitted in partial satisfaction of the

requirements for the degree Doctor of Philosophy

in Geography

by

Kellie Ann Uyeda

Committee in charge:

Professor Douglas Stow, Chair

Professor John O'Leary

Professor Allen Hope

Professor Christina Tague

Professor Dar Roberts

September 2015

The dissertation of Kellie Ann Uyeda is approved.

_____

Dar Roberts

_____

Christina Tague

_____

Allen Hope

_____

John O'Leary

_____

Douglas Stow, Committee Chair

July 2015

Spatial and temporal variation in biomass accumulation in southern California chaparral

ACKNOWLEDGEMENTS

I would like to first thank my committee for their guidance and support. In particular, I appreciate the countless hours Doug invested to help me develop my ideas and grow as a researcher. I am grateful for the opportunity to have spent many days in the field learning from John's extensive knowledge of chaparral systems. Allen's thoughtful comments in his 'Wildland Fires' seminar have stuck with me over the years. Dar and Naomi have provided me with valuable feedback and insightful questions through the process of developing my proposal and dissertation, and I am grateful for how they have helped shape my research. In addition, I am grateful to Philip Riggan, who was the Principal Investigator on the grant that funded much of my dissertation, and whose ideas helped shape the initial direction of my research.

My husband Frank is at least partially responsible for me even considering that pursuing a doctorate might be a reasonable life direction. We have had some great adventures together, and our latest adventure in parenting has been the best yet. His love and encouragement have kept me going when I felt stuck, and I am thankful to be sharing life together.

My twin boys Darrell and Owen arrived in the last year of my program, and they have been a huge blessing. I have fond memories of measuring shrub growth rings on my computer while my tiny babies slept on my lap. I am overjoyed to be the mother of these awesome little people.

I am also grateful to my mother, who encouraged me to explore the natural world from an early age. When I was a child, she amazed me by keying out the strange plant we had found and telling me its name: *Marah macrocarpus* (wild cucumber). I am reminded of this

experience and my mother's love for nature whenever I see this plant, and hope that I can share the same love and excitement with my own children. I am also thankful for my father, who helped me with countless science projects as a child, and has been encouraging and supportive of my latest five year science project.

I am also grateful to the many fellow graduate students who made the long doctoral journey more worthwhile. Thank you to Denise Goerisch, Zia Salim, Ryan Bart, Jaime Rossiter, Sarah Wandersee, Alex Zvoleff, Nicole Simons, Cindy Tsai, Kris Taniguchi, Crystal English, Yelena Granovskaya, Laurel Hanscom, and many others for sharing life with me during my time in the Geography department. I consider myself fortunate to have such bright and talented people as my friends. I am particularly grateful to Ian Schmidt, who spent many long hours in the field and the lab with me as he worked on his master's research on a related topic.

I would like to thank the SDSU and UCSB Geography staff, and in particular, Allison Bailund, Harry Johnson, and Pete Coulter, for all the times they have helped me stay on track with their prompt and helpful answers to my questions.

I am thankful for the members of the Coast Vineyard church community and the Mira Mesa home group for praying for me and encouraging me throughout this long process. I am also grateful to the many hospitable friends from church, UCSB, and SDSU, who let me stay in their spare bedrooms and on couches while I was constantly traveling back and forth between Santa Barbara, Los Angeles, and San Diego. My friends Jamie and Eric Reichling also generously provided use of their tools and garage while I sanded hundreds of shrub cross sections.

A huge number of friends from all areas of my life made time to help me in the field. I might still be out in the field trying to measure the last remaining plots if it were not for the overwhelming support of my friends. The full list of people who helped with field work includes (in roughly chronological order): John O'Leary, Ian Schmidt, Diane Rachels, Callie Riggan, Phil Riggan, Alissa Brown, Frank Uyeda, Julia Jesu, Benito Lo, Michael Beland, Bonni Corcoran, Drew Smith, Emanual Storey, Justin McCullough, Kyle Walsh, Yelena Granovskaya, Allison Clark, Jeremy Schichtel, Lesley Handa, Megan Hartfelder, Kurt Hartfelder, Rebecca Elliott, Aly Lewis, and Doug Stow. In addition, I am grateful to Mike Oxford from USFS for arranging for field site and facilities access at San Dimas Experimental Forest, and to John Truett, Talbot Hayes, and Jason Kraling from the USFS for arranging for field site access at Long Canyon.

Funding for this project was provided by the USDA Forest Service through American Recovery and Reinvestment Act Agreement No. 10-JV-11279701-10: Airborne remote sensing to enable hazardous fuels reduction, forest health protection, rehabilitation and hazard mitigation activities on Federal lands. I am also grateful to the SDSU Geography department and the William and Vivian Finch Award in Remote Sensing for providing additional financial support.

VITA OF KELLIE ANN UYEDA
July 2015

EDUCATION

Bachelor of Science in Environmental Systems, emphasis in Ecology, Behavior and Evolution, University of California, San Diego, June 2006
Master of Science in Ecology, San Diego State University, May 2010
Doctor of Philosophy in Geography, San Diego State University and University of California, Santa Barbara, July 2015 (expected)

PROFESSIONAL EMPLOYMENT

2006 - 2010: Research Associate, Tijuana River National Estuarine Research Reserve
2007 – 2008: Teaching Associate, San Diego State University, General Biology Lab
2007-2009: Research Field Assistant, San Diego State University, Multiple Species Conservation Plan monitoring
2010 – 2014: Graduate Research Assistant, San Diego State University
January 2014 – May 2014: Teaching Associate (Instructor of Record), San Diego State University, Intermediate Remote Sensing of the Environment

PUBLICATIONS

Uyeda, KA, D. Deutschman, J. Crooks. 2013. Abiotic Limitation of Non-Native Plants in the High Salt Marsh Transition Zone, Estuaries and Coasts. 36 (6): 1125-1136

Chen, X.; N. Emery, E. Garcia, E. Hanan, H. Hodges, T. Martin, M. Meyers, L. Peavey, H. Peng, J. Sainz, K. Uyeda, S. Anderson, C. Tague. 2013. Perspectives on disconnects between scientific information and management decisions on post-fire recovery in Western US, Environmental Management. 52 (6), 1415-1426

Uyeda KA, Stow DA, Riggan PJ. 2015. Tracking MODIS NDVI time series to estimate fuel accumulation. Remote Sensing Letters. 6 (8) 587-596

Uyeda KA, Stow DA, O'Leary JF, Schmidt, IT, Riggan, PJ. 2015. Spatial variation of fuel loading within varying aged stands of chaparral. Applied Vegetation Science. (in review)

AWARDS

NOAA National Estuarine Research Reserve Graduate Research Fellow, "Using soil salinity and soil moisture to inhibit invasive species at the upland-high marsh ecotone" $40,000, June 2008 - May 2010

Department of Geography Citizenship Award (2013)

SDSU Graduate Student Travel Fund Award (2014)

William and Vivian Finch Scholarship in Remote Sensing (2013)

FIELDS OF STUDY

Fire ecology, multi-temporal remote sensing, landscape ecology, chaparral ecology

ABSTRACT

Spatial and temporal variation in biomass accumulation in southern California chaparral

by

Kellie Ann Uyeda

Wildfires are a common occurrence in chaparral shrublands, and post-fire patterns of biomass accumulation are important for understanding ecosystem productivity and fuel available for future fires. In this research, I examine patterns of biomass accumulation in southern California chaparral shrublands at early and late stages of post-fire recovery using a combination of detailed field work and remote sensing. Using field measurements of a site with adjacent stands of varying ages and high spatial resolution imagery, I examine patterns of species composition and associated levels of biomass to characterize long-term patterns in biomass accumulation. I also evaluate the potential for utilizing shrub growth ring widths to track annual biomass accumulation in the first decade of post-fire recovery, and test for the relationship between biomass and spatial variation in factors related to the energy and water balance. In addition, I examine the potential for extending the use of shrub growth rings to track biomass across larger spatial extents using satellite-based growth metrics. The study of stands of varying ages reveals that biomass shows substantial variation even within stands of the same age, and that species composition is different in younger stands of chaparral compared to the more mature stands. In the study of growth rings, I find that while

measuring growth rings widths is a valuable method for tracking biomass accumulation in the first decade following a fire, there is no apparent relationship between biomass and factors related to the energy and water balance. Annual biomass growth, as estimated from shrub growth ring widths, shows a promising relationship with satellite-based metrics of annual growth, indicating the potential for further study of the relationship over larger spatial extents.

TABLE OF CONTENTS

LIST OF FIGURES

LIST OF TABLES

Chapter 1: Introduction

A. Motivation for Research

Wildfires play an important role in the global carbon cycle. They quickly release carbon that might not accumulate to pre-fire levels due to changes in climate, vegetation type, or fire-return interval (Kaye et al. 2010). With more extreme weather predicted in the future due to accelerated climate change (Easterling et al. 2000), it is becoming increasingly important to understand major disturbance events such as fires and drought that are associated with these extreme weather patterns (Breshears and Allen 2002).

Recent massive wildfires in southern California chaparral shrublands have had major economic and societal costs, and wildfires of similar scale are to be expected in the future (Keeley et al. 2009; Keeley et al. 2004). Patterns of biomass accumulation are important for understanding ecosystem productivity following a fire, which is closely related to the fuel available for future fires and their ecological fire effects (Riggan et al. 1988). An improved understanding of fuel accumulation could help inform management of wildfires and resource allocation.

In southern California chaparral shrublands, wildfires typically occur as intense crown fires, with behavior influenced by meteorological conditions (i.e. high temperatures, low humidity, high winds) (Dennison et al. 2008), terrain and biomass levels. These evergreen sclerophyllous shrubs form thick, nearly impenetrable stands which are almost completely consumed during fires. The first three to four years following a fire are characterized by an abundance of herbaceous and suffrutescent vegetation, after which shrubs become dominant and return to pre-fire cover levels within ten to fifteen years

(Hanes 1971; McMichael et al. 2004). This recovery process can be disrupted by drought stress (Hope et al. 2007) and is spatially variable (Kinoshita and Hogue 2011). Patterns of biomass accumulation are important for understanding future fire patterns, as well as ecosystem recovery and carbon sequestration.

While shrub cover returns to pre-fire cover levels within the first 10 – 15 years, the amount of total stand biomass continues to increase with time (Riggan et al. 1988). The rate of this accumulation declines with time, but there appears to be positive net accumulation at least until an age of approximately 40 years. After this time, vegetation appears to reach a steady state, with net accumulation rates of zero (Black 1987). Although live shrubs continue to accumulate fuels over long time periods, fine fuels (live stems over 6.3 mm or dead stems over 76 mm) are most important for fire propagation and are considered available fuel (Burgan and Rothermel 1984). Available fuel does increase with total biomass, but the relationship appears non-linear (Regelbrugge and Conard 1996).

In a broad sense, the total amount of dead fuel also increases with time as branches die back due to light limitation (Mahall and Wilson 1986) or drought stress (Davis et al. 2002), or as entire shrubs die during stand development (Schlesinger et al. 1982). However, the proportion of dead fuel even within a single species is highly variable, and stand age is likely not the most important factor in determining the proportion of dead fuel (Paysen and Cohen 1990). Dead remnant stems from the last fire are also an important source of dead fuel. In young stands without high live biomass, these dead remnant stems may represent a high percentage of total biomass (Regelbrugge and Conard 1996).

Chaparral vegetation is very dense and nearly impassable to humans. Remote sensing provides valuable information on vegetation condition across large areas, and recent

studies have used a variety of methods for characterizing southern California shrublands. These include object based image analysis (OBIA) (Stow et al. 2008) , satellite-based spectral vegetation indices (SVIs) (Kinoshita and Hogue 2011; McMichael et al. 2004) and mixture models (Riaño et al. 2002b; Roberts et al. 2006). Although remote sensing studies provide information on post-fire recovery at a much larger extent than could be accomplished using field methods alone, deriving accurate biomass measurements from remotely sensed data is difficult (Lu 2006), and many studies of post-fire recovery either don't include field data (Kinoshita and Hogue 2011), or provide only cover data (van Leeuwen et al. 2010).

Fuel properties in chaparral change through time in ways that are often not straightforward or linear, and remote sensing provides a valuable method for studying these patterns. I am broadly interested in how chaparral fuel properties change at both short and long time scales. In this research, I measured and analyzed annual growth rates at short time scales, and tested the potential for regional mapping of chaparral growth. At longer time scales, I explored differences in fine-scale spatial patterns of biomass. In the three components of my dissertation, I used a novel combination of detailed field measurements and remote sensing techniques to investigate spatial and temporal changes in chaparral fuel properties.

B. Overview of chapters

In Chapter 2, "Spatial variation of fuel loading within varying aged stands of chaparral", I performed detailed field sampling to measure biomass in adjacent 7-, 28-, and 68-year-old stands of chaparral in San Diego County. I used high-resolution imagery to classify each stand into species groups using an OBIA approach, then mapped biomass using coefficients

for the average biomass per area for each species group and stand age. I address the following research questions: 1) How do stand-level biomass and percentage of dead material in chaparral vary as a function of stand age? 2) How do the landscape properties of aggregation, species composition, and patch size vary as a function of stand age?

In Chapter 3, "Chaparral growth ring analysis as an indicator of stand biomass development", I conducted additional detailed field sampling of biomass in an 11-year-old stand of chaparral in San Dimas Experimental Forest in Los Angeles County. I collected hundreds of shrub cross-sections from field plots and measured the annual growth rings. Using equations based on field measurements of shrub biomass and stem area, I estimated incremental biomass accumulation for each plot in years 5 – 11 of post-fire growth. I use this information to address the following research questions: 1) Do measurements of shrub growth ring change increments provide a useful metric of biomass accumulation? 2) How does biomass accumulation of recovering shrubs, measured as the change in growth ring diameter, vary with differences in annual precipitation? How does this response vary with time-since-fire? 3) How do spatial patterns of shrub biomass accumulation vary with factors related to site energy and water balance (solar irradiation and flow accumulation)? Chapter 4, "Combining ground-based measurements and MODIS-based spectral vegetation indices to track biomass accumulation in post-fire chaparral" expands on the work of Chapter 3. I examine the relationship between seasonal growth metrics calculated based on MODIS-based SVIs and patterns of annual biomass accumulation estimated using measurement of annual growth ring diameters. I address the following research questions: 1) Which MODIS-based metrics of annual growth are most closely related to ground-based measurements of annual biomass accumulation in chaparral obligate seeder shrubs and what

is the degree of temporal co-variability? 2) Is the relationship between MODIS-based growth metrics and biomass sufficiently strong to indicate a potential for mapping biomass growth at regional scales?

Chapter 2: Spatial variation of fuel loading within varying aged stands of chaparral

A. Abstract

In this study, I conducted a field study of adjacent stands of 7-, 28-, and 68-year-old chaparral in San Diego County, CA to address the following research questions: How do stand-level biomass and percentage of dead material in chaparral vary as a function of stand age? How do the landscape properties of aggregation, species composition, and patch size vary as a function of stand age? I sampled and estimated above-ground biomass in 8 m x 8 m field plots. Each stand was classified into species groups using high-resolution imagery. After establishing coefficients for the average biomass per area for each species group and stand age using field data, I estimated biomass in 30 random plots in each stand age using the classified map. I also estimated biomass using pooled coefficients (the average of the 28- and 68-year-old biomass per area). I calculated landscape metrics in six 60 m x 60 m study areas in each stand age. While there is a statistically significant pattern of higher biomass in the older stands when using age-specific biomass coefficients, there is no statistical difference between the 28- and 68-year-old stands using the more conservative pooled coefficients. Both approaches reveal a wide range in biomass in all age classes. I was not able to map dead biomass with sufficient accuracy to measure age-related differences, but no differences in the two older stands were obvious in the field. There are no significant differences in landscape metrics between the two older stands, and the differences observed in the younger stand might be partially due to aspect differences. My approach of using a combination of field plots and classification of high-resolution imagery is a valuable method

for enlarging the effective study area in chaparral, and allowed me to better measure how widely biomass varies across the study area.

B. Introduction

In southern California chaparral shrublands, wildfires typically occur as intense crown fires, with behavior influenced by meteorological conditions (i.e. high temperatures, low humidity, high winds), terrain and biomass levels. These evergreen sclerophyllous shrubs form thick, nearly impenetrable stands in which most above-ground biomass is completely consumed during fires. The first three to four years following a fire are characterized by an abundance of herbaceous and suffrutescent vegetation, after which time shrubs become dominant and return to pre-fire cover levels within ten to fifteen years (Hanes 1971; Keeley and Keeley 1981; McMichael et al. 2004). While shrub cover returns to pre-fire levels fairly rapidly, the amount of total above-ground biomass continues to increase with time (Riggan et al. 1988). The rate of this accumulation declines with time within the first two decades of recovery, but there appears to be positive net accumulation at least until an age of approximately 40 years (Black 1987; Rundel and Parsons 1979). After 40 years, vegetation biomass tends to reach a steady state, with net accumulation rates of zero (Black 1987). These patterns of biomass accumulation are important for understanding ecosystem productivity following a fire, which is closely related to the fuel available for future fires and their ecological fire effects (Riggan et al. 1988).

Although broad-scale patterns of fire frequency are not necessarily related to fuel age (Keeley and Zedler 2009; Moritz et al. 2004), fuel characteristics such as total fuel loading and percent moisture are among the important factors in determining fire spread success (Weise et al. 2005). The contribution of dead fuel is thought to be particularly important for

fire spread since the low moisture levels of dead fuel may allow fire to spread through live fuels (Countryman and Dean 1979).

In a broad sense, the total amount of dead fuel increases with time as branches die back due to light limitation (Mahall and Wilson 1986), drought stress (Davis et al. 2002) or pathogens (Riggan et al. 1994), or as entire shrubs die during stand development (Riggan et al. 1988; Schlesinger et al. 1982). However, the proportion of dead fuel is highly variable. Even for a single species and over large areas, stand age is likely not the most important factor in determining the proportion of dead fuel (Paysen and Cohen 1990). In a study in the Mediterranean Basin, the proportion of dead biomass showed a peak around ten years following a fire, then declined with time as species that retain high levels of dead biomass were replaced by species retaining lower levels of dead biomass (Baeza et al. 2011). Dead remnant stems from the last fire are also an important source of dead fuel. In young stands without high live biomass, these dead remnant stems may represent a high percentage of total biomass (Regelbrugge and Conard 1996). Large remnant stems, when burned, may not contribute greatly to stand ignitability or fire behavior, but would contribute to overall energy release and some ecological fire effects such as soil heating.

Chaparral biomass accumulates over long time scales, and fuel properties can be highly variable. Since the time scales of interest are so long, it is usually impossible to follow a single stand through time. Instead, researchers typically take measurements from multiple stands to reconstruct a chronosequence of temporal change in fuel. Due to the large areas commonly consumed by wildfires, stands that make up each age group are often composed of heterogeneous vegetation, soil types, and terrain characteristics. Also, areas that remain

unburned for long periods of time may fundamentally differ in their landscape characteristics from those that frequently burn or have recently burned.

Previous studies have found chaparral biomass to exhibit a high degree of fine-scale spatial variability (Black 1987). Fine-scale variations in fuel could drive important fine-scale variations in fire behavior, although more data are needed to link fine-scale fire behavior patterns to the broad scales of interest to fire managers (Hiers et al. 2009). One source of variation is due to the species composition of a given stand. *Adenostoma fasciculatum* (chamise), the most common chaparral shrub in California (Hanes 1971), has been relatively well studied in terms of shrub-scale fuel properties. It has fine, needle-like leaves, with a high proportion of small-diameter stems (Countryman and Philpot 1970). It retains dead stems in the canopy, which contributes to increased fire intensity (Schwilk 2003). The percentage of dead biomass is highly variable even in stands of the same age, and might be related to site productivity (Countryman and Philpot 1970; Riggan et al. 1988). *A. fasciculatum* is commonly found on south-facing slopes (Hanes 1971). *Quercus berberidifolia* (scrub oak) is also often present in California chaparral, typically on north-facing slopes (Hanes 1971). It has relatively broad leaves, and accumulates only low levels of standing dead biomass (Riggan et al. 1988). It has a comparatively lower proportion of small-diameter stems (Riggan et al. 1988) and is usually taller, with higher fuel volume than *A. fasciculatum* (Green 1970). Regardless of this variation, chaparral fuels often have been mapped at relatively coarse scales, with groupings of fuel types rather than plant-specific measurements of biomass (Riaño et al. 2002a).

The objective of this study is to measure the fine-scale changes in fuel properties that occur over long time periods as southern California chaparral ages. The general study

location has previously served as the field site for a study of chaparral community development, and the published field data are available for comparison (Riggan et al. 1988). The fuel ages in the study sites vary as the result of prescribed or experimental fires, and vegetation composition, soil properties, and topographic characteristics can be expected to be similar, even though stand ages differ. Reducing the effect of spatial variability by constraining this project to a small study area enables me to more closely quantify fine-scale differences in above-ground biomass as a function of stand age. While the use of a small study area may appear to reduce the broader applicability of the results, the selected site is representative of typical southern California chaparral. Understanding how fuel properties such as total and dead biomass and their spatial arrangement across the landscape change with age has the potential to inform fuel management policies.

I address the following research questions using detailed measurements of chaparral field plots: (1) How do stand-level biomass and percentage of dead material vary as a function of stand age? (2) How do the landscape properties of aggregation, species composition, and patch size vary as a function of stand age?

C. Methods

1. Study site

The site for this study is located near Kitchen Creek Road on southern Laguna Mountain in San Diego County, CA (Figure 1). Chaparral there experiences a typical Mediterranean-type climate with hot, dry summers, and cool, wet winters. The soils are classified as being in the Bancas series which are fine loamy, mixed, mesic, and mollic haploxeralfs derived from quartz diorite and mica schist (http://websoilsurvey.nrcs.usda.gov/, accessed 19 Dec 2014). Average annual precipitation is 66 cm per year (http://www.prism.oregonstate.edu/,

accessed 4 April 2014). *Adenostoma fasciculatum*, a facultative seeder and *Quercus berberidifolia*, an obligate resprouter, are dominant species on the site, although *Arctostaphylos glandulosa* and *Ceanothus perplexans* (formerly *Ceanothus greggii var. perplexans*) are also commonly found.

The entire study area burned in 1944. Three strips were burned as part of an experimental burn in 1979, then additional areas were burned in the early 1980s, creating one burned area approximately 300 m north of another burned area on a background of older vegetation in the study area designated "Kitchen Creek" (Dougherty and Riggan 1982; Riggan et al. 1988). In 2005, a prescribed burn was conducted on the nearby site called "Long Canyon." This created three stand ages (68 years, approximately 28 years, and 7 years) within one kilometer of one another at elevations ranging from 1430 m to 1520 m. While minimal differences in aspect exist between the two older, mostly east-facing sites, the 7-year-old site is more southeast-facing.

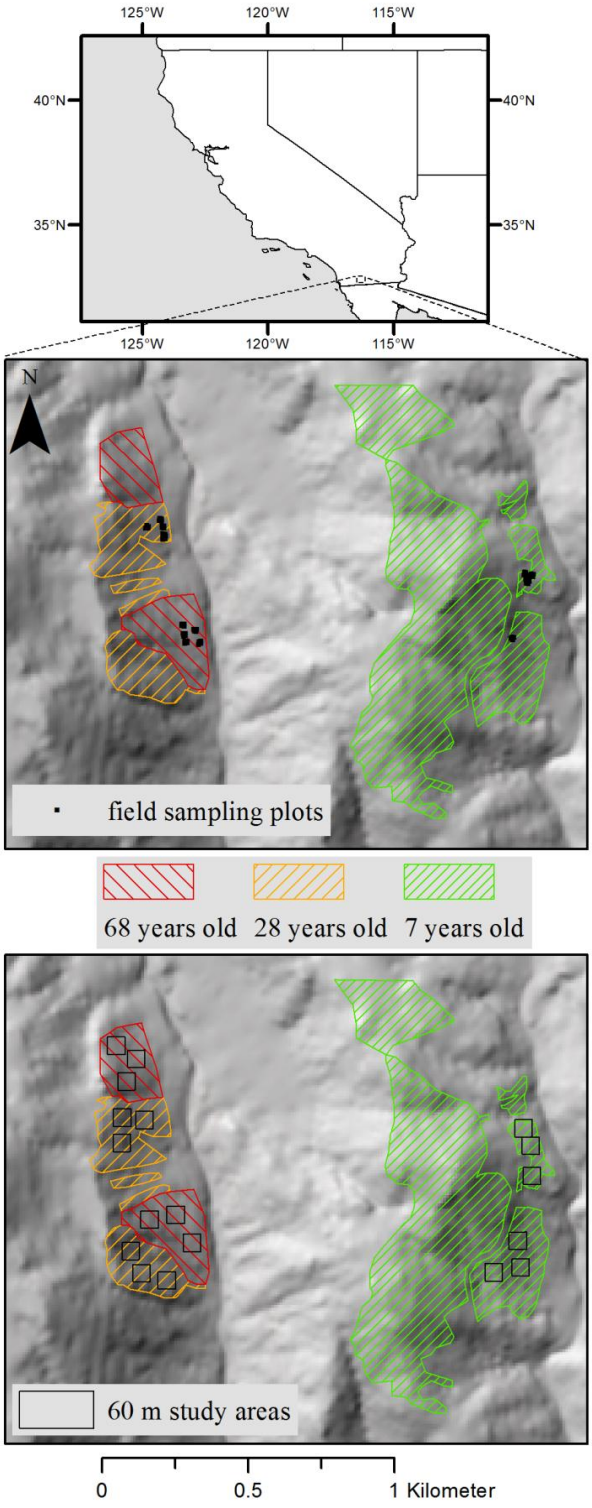

Figure 1: Overview of field sites and 60 m x 60 m study areas at Kitchen Creek (western burn areas) and Long Canyon (eastern burn area). Fire perimeters at Kitchen Creek were digitized based on imagery collected in 1985.

2. Field methods

The research goals for this portion of the study are to measure basal area and above-ground biomass, establish regression relationships between these two measured variables, estimate above-ground biomass based on basal area measurements, and compare live and dead above-ground biomass in a range of stand ages. Five 64 m^2 (8 m x 8 m) plots encompassing the range of variability of the study area were selected from each of the three age classes (68, 28, and 7 years) for a total of 15 plots. Shrub cover in the two older areas was extremely dense, and I was only able to access the plots in a timely fashion because a trail was cut through the study area by a fire crew from the US Forest Service. All plots in the Kitchen Creek area were located within 40 m of this trail. Plot boundaries were recorded in the field using Trimble GeoXM handheld Global Positioning System (GPS) unit with a post-processed accuracy of 1 to 3 m. I measured all shrub stems 0.4 cm or greater in diameter within the plots at 10 cm above the ground using digital calipers and recorded the species of the stem and whether it was live, dead, or charred. On irregularly shaped stems, I recorded the minimum and maximum stem diameters to determine the average stem diameter. Shrubs that were partially outside the plot were measured and included in plot estimates if more than half the basal stem area of the shrub was within the plot. Live stems were identified by the presence of green leaves, so stems that were mostly dead were still counted as live if green leaves were present. I recorded stems from each shrub separately, although in some cases (most often with *Q. berberidifolia*) it was difficult to conclusively determine to which shrub the stems belonged.

I harvested live, dead, and for the 7-year-old area, charred stems from the most abundant species (*A. fasciculatum, Q. berberidifolia, A. glandulosa, C. perplexans*) near the sampling

plots to determine field weight and basal diameter. I typically sampled one species per day and selected one shrub per day to serve as a representative sample to estimate the ratio of dry-to-wet weights. This representative shrub was brought to the lab where I separated it into small (< 0.5 cm), medium (0.5 cm to 2 cm) and large (>2 cm) diameter fractions. I weighed each size fraction and subsampled it to determine water content. Samples were dried to a constant mass in a drying oven at 100 ˚C. I determined the total shrub water content by applying the appropriate water content value to the biomass of each shrub fraction to calculate an average water content scaled by size fraction. This value was then applied to all shrubs sampled on that day. This sampling took place mostly in the fall and early winter seasons from 2011-2013.

I calculated coefficients for the relationship of dry above-ground biomass (AGB) as a power function of basal area (BA) with a bias correction applied (Baskerville 1972; Sprugel 1983):

$$\mathbf{AGB} = \mathbf{B_0}(\mathbf{BA})^{\mathbf{B_1}}\mathbf{e}^{\mathbf{0.5\,s}} \quad \textbf{Equation 1}$$

where s is the residual mean square, B_0 is the proportionality coefficient, and B_1 is the scaling exponent.

In order to optimize time spent in the field, I generated species and age-specific equations for each species in the burned areas where they were most abundant. For example, scrub oak was only occasionally found in the 7-year-old area, so I used the equation from the 28-year-old area rather than generating a new equation. I also generated a generic equation for each age class using the pooled measurements across all species to provide an estimate for less abundant species. I calculated above-ground biomass for entirely dead shrubs that could not be identified by species using the generic dead shrub equation for the appropriate burn year. Charred stems were only occasionally found in the older stands, so I

estimated charred biomass in these areas using half the value given by the appropriate equation for dead biomass. I was able to use a species specific equation to calculate shrub biomass for at least 90% of the total basal area present in each plot. Although the number of individual stems and shrubs from which those stems were harvested are presented, the regression relationships are based only on the basal area measurements of individual stems. I made every effort to sample shrubs from the full range of basal area values found in the field plots, but it was not always possible to locate large enough shrubs for the destructive sampling. A maximum of 4% (and usually much less) of all stems in the field plots were so large as to require an extrapolation of the regression equation to estimate biomass.

3. Image Classification

Although field sampling is necessary to estimate biomass values, it is very time consuming and logistically challenging within the dense canopy and steep slopes of chaparral to collect a sample size large enough to adequately characterize the range of variability found in the study area. In order to characterize the fuel properties of each age class, I classified imagery from the 68- and 28-year-old age classes of chaparral using color (RGB) aerial imagery collected by Near Earth Observation Systems (NEOS) LTD in June 2012 using a 21 megapixel digital camera. The imagery was geometrically corrected using control point based warping and mosaicked using nearest neighbor resampling to create a single image of the entire Kitchen Creek study area. The ground sample distance (GSD) of the corrected data set is 4 cm. In addition, a Normalized Difference Vegetation Index (NDVI) product from May 2012 color infrared imagery having a nominal 50 cm GSD was also used as an input for the classification. NDVI is calculated as the difference of near infrared and red digital number values divided by the sum of those values.

I utilized eCognition, an object-based image analysis (OBIA) software package, for image-based classification of vegetation types (eCognition Developer 8.9, http://www.ecognition.com/). This approach allows the user to segment an image into groups of adjacent pixels (objects) and then classify the objects according to a classification scheme (described below) and user-defined rules. I used an iterative segmentation/classification approach, re-segmenting several times to create objects of the appropriate size for the class of interest. A multiresolution segmentation algorithm with scale parameters of 10 and 15 was implemented, as well as the chessboard segmentation algorithm with object sizes of 1 and 10. After each round of segmentation, I used properties such as texture, brightness, color, adjacency, and NDVI to classify the objects in the class of interest, then merged the unclassified objects so they could be re-segmented with appropriate parameters for the next class of interest.

I collected calibration/validation samples from 1 m x 1 m plots in the Kitchen Creek study area (68- and 28-year-old vegetation) along the trail using the Trimble GeoXM GPS unit. Eighteen of the plots were used to train the classifier, and 42 were used for validation. Although I made minor manual corrections to the vegetation type maps in the primary study area, the accuracy assessment was based on the uncorrected classification results.

While some of the 7-year-old age class was covered by the NEOS imagery, the coverage was not sufficient to classify vegetation within the entire area. Thus, the 2012 50 cm CIR imagery was used as input to the eCognition routines for this area. NEOS imagery was used as a reference for training purposes.

Initially, the image-based classification scheme consisted of broadleaf, *A. fasciculatum*, *A. glandulosa*, subshrub, bare, and dead categories. I later combined *A. fasciculatum* and *A.*

glandulosa into a single "narrowleaf" category due to the low numbers of *A. glandulosa* and lower biomass per area found in that species relative to *Q. berberidifolia*. Although *A. glandulosa* does not have narrow leaves, the category was named for the narrow leaves of *A. fasciculatum.* I also aggregated the biomass measured in the field-based on these same category groupings. The broadleaf category mostly consisted of *Q. berberidifolia* and *C. perplexans*, although the less common species *Ceanothus leucodermis, Cercocarpus betuloides, Quercus agrifolia, Rhamnus ilicifolia, Rhus ovata, Rhus trilobata,* and *Ribes indecorum* were also included. The subshrub category was mostly composed of *Salvia apiana,* but also included small amounts of *Trichostema lanatum, Keckiella ternata, Hazardia squarrosa,* and *Eriogonum fasciculatum.* The bare category was mostly composed of granite outcroppings in the 28-and 68-year-old areas, and a combination of granite outcroppings and bare ground in the 7-year-old area. The dead category included only shrubs that were entirely dead. Dead biomass attached to living shrubs was included within the appropriate species group. I was unable to classify dead cover in the 7-year-old area due to the relatively coarse resolution of the imagery and small quantity of dead material in this area.

Vegetation cover percentages of each field plot were extracted from the image classification product. Although I made every effort to set up square plots in the field, the difficulty of moving through dense chaparral sometimes resulted in slight geometric distortions to the desired square 64 m^2 plots. There was also some error associated with the plot boundaries recorded using the GPS unit in the field. I was able to correct for this error in several of the plots because I placed bright ground targets above the canopy, which were clearly identifiable in the high spatial resolution imagery.

4. Data analysis

I calculated biomass per m^2 using biomass (measured in the field) and species category cover (measured using imagery classification). I used the average biomass per m^2 of the two plots from each age and species category with the highest field measured biomass for a given species category. Since the plots were composed of a mixture of species, samples of some plots were not representative of the species category of interest. In order to reduce the error associated with these plots, I based the calculation on only the plots in which the species category of interest was abundant. While this unfortunately resulted in a reduced sample size, it is the result of a field sampling strategy that involved collecting highly detailed biomass information over relatively large (64 m^2) plots. The large plot size allowed me to have greater confidence in geolocation accuracy and biomass estimates within each plot, but due to the time intensive nature of this approach, I was not able to sample a large number of plots dominated by each of the species categories of interest. In order to provide a more cautious estimate of biomass, I also calculated the average biomass per m^2 for the combined 68- and 28-year-old areas. I did not include the 7-year-old area in this calculation because these values were much lower than those found in the older burn areas.

The first research question —How does stand-level biomass vary as a function of stand age? — was addressed using the classified map of biomass. I selected six 60 m x 60 m study areas within each age class for a total of 18 large study areas. I selected this size because it was the largest area that would fit in the burn perimeters of the 7-year-old area. I clustered the study areas into three northern and three southern study areas, each separated by at least 200 m (Figure 1). The aspect of the 60 m x 60 m study areas, based on a 10 m spatial resolution digital elevation model, is shown in Figure 2. In each of these study areas, I

randomly selected five 8 m x 8 m plots for a total of 30 plots per burn age (90 plots total). I calculated the total biomass using the age-specific coefficients of broadleaf, narrowleaf, subshrub, and dead biomass determined previously. This is based on the assumption that biomass is uniform for a given age and species group. To determine if differences in biomass were robust to possible error in the age-specific coefficients, I also calculated an estimate of biomass using the averaged coefficients for the 68- and 28-year-old age classes. I tested for biomass differences in the three age classes with one-way ANOVA (n = 30).

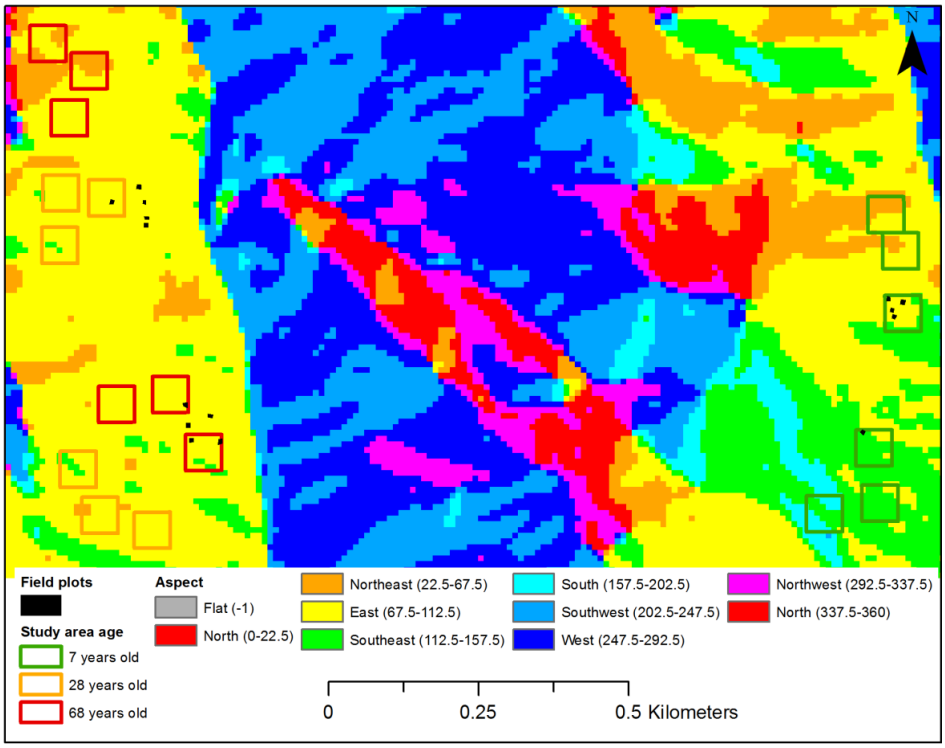

Figure 2: Map of aspect within each of the 60 m x 60 m study areas and 8 m x 8 m field plots, generated using a 10 m spatial resolution digital elevation model. Note that while nearly all the 8 m field plots face directly east, the aspect of the 60 m study areas range from directly south to northeast.

I addressed the second research question —How do the landscape properties of aggregation, species composition, and patch size vary as a function of stand age? — by comparing landscape metrics derived from vegetation-class patches from the 18 large (60 m

x 60 m) study areas. The aggregation index is calculated by dividing the cell adjacencies of a given class by the total number of possible cell adjacencies for that class. It is given as a percentage, such that a given class clumped in a single, compact patch would have a value near 100. I examined species composition by calculating the percent cover of each species group. Patch size for each species group was calculated using the area-weighted patch mean size, in which each patch is weighted by its proportional area representation. I calculated these metrics for each species group using a 50 cm resolution version of the vegetation classification from the 60 m x 60 m study areas in each of the three age classes with the software program Fragstats (version 4.1, http://www.umass.edu/landeco/research/fragstats/fragstats.html). Since the vegetation map of the 7-year-old age class was produced using 0.5 m imagery, I reduced the resolution of the 68- and 28-year-old age classes (originally 4 cm) to match this lower resolution of 50 cm using nearest neighbor resampling. I compared the difference in these metrics in the three age classes with one-way ANOVA (n=6). In order to more closely examine the differences in the 68- and 28-year-old age classes, I also calculated the same metrics using the original resolution (4 cm) vegetation classification. I compared the landscape metrics for the two age classes using a series of t-tests (n=6).

D. Results

1. Stand-level biomass

Regressions of biomass as a function of basal area for the four chaparral species are presented in Figure 3, and regression coefficients are shown in Table 1. The R^2 values for the biomass equations are high and range from 0.82 to 0.97. The R^2 values for dead biomass are somewhat lower, and range from 0.65 to 0.96. The covariation between biomass and

basal area is highest in 68-year-old *Q. berberidifolia* and lowest in 7-year-old *A. fasciculatum.*

Biomass measurements from the field survey range from 7.5 kg m-2 in one of the oldest plots to 1.1 kg m-2 in one of the youngest plots (Table 2). The highest biomass values are found in the 68-year-old stand, particularly in plots dominated by *Q. berberidifolia*. Despite these much higher values in the oldest plots, there is considerable overlap in the total biomass values in the 68- and 28-year-old plots. Total biomass values are much lower in the 7-year-old plots, as expected. Charred stems are found only occasionally in the older areas, but are abundant in the 7-year-old area. Charred stem biomass ranges from about one-third to nearly equivalent to the amount of post-fire growth in these plots, although the regression relationship for calculating charred stem biomass exhibits a high degree of scatter, meaning that actual values of charred biomass may vary substantially from what I estimated.

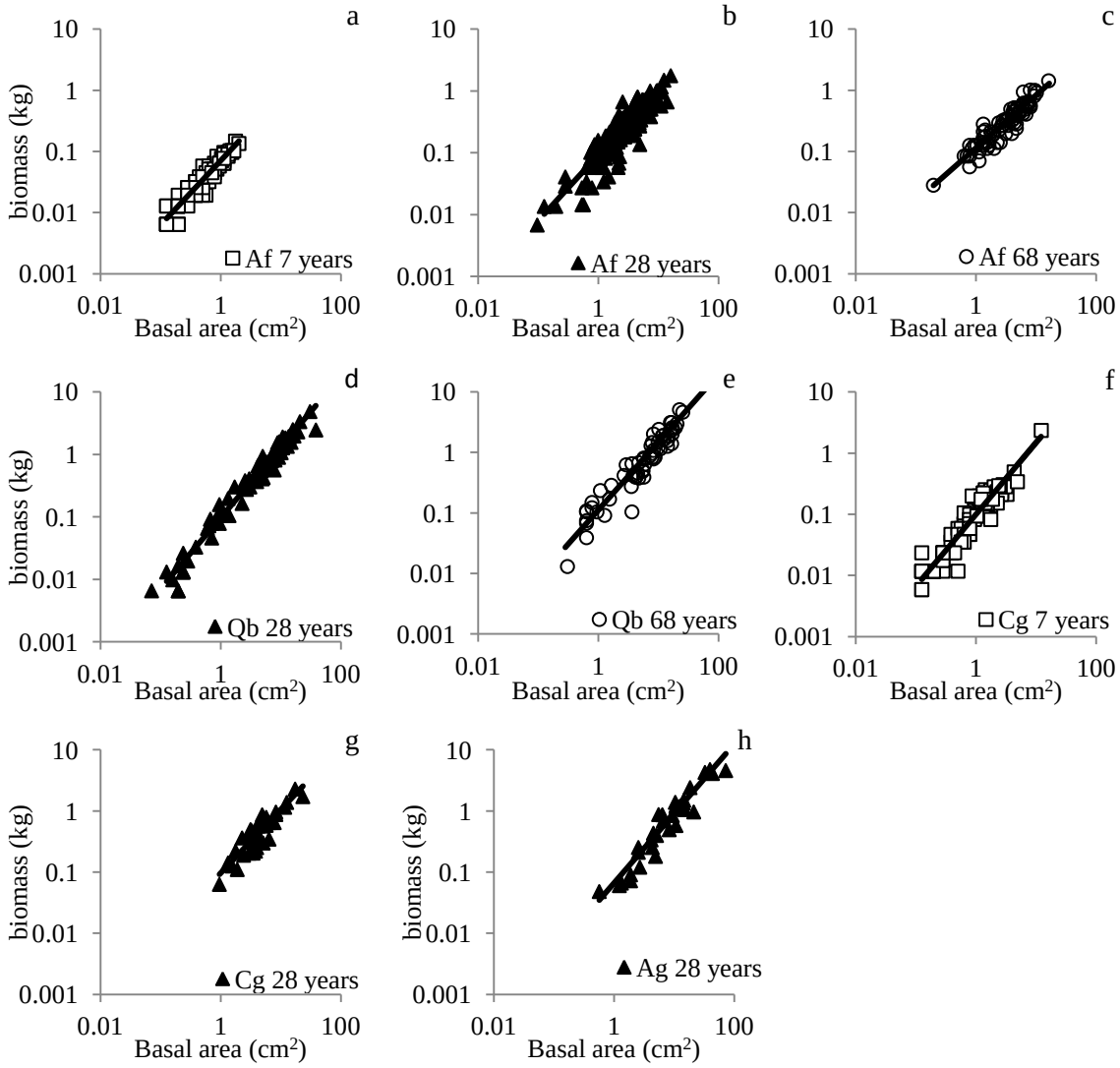

Figure 3: Regressions of biomass as a function of basal area for a) *Adenostoma fasciculatum* at 7-years-old, b) *A. fasciculatum* at 28-years-old, c) *A. fasciculatum* at 68-years-old, d) *Quercus berberidifolia* at 28-years-old, e) *Q. berberidifolia* at 68-years-old, f) *Ceanothus greggii* at 7-years-old, g) *C. greggii* at 28-years-old, and h) *Arctostaphylos glandulosa* at 28-years-old

Table 1: Regression coefficients of stem biomass (kg) as a function of basal area (cm^2).

Live biomass

species	stand burn age	max diameter (cm)	min diameter (cm)	$B_0*e^{0.5s}$	B_1	R^2	stems / shrubs
A. fasciculatum	68	4.6	0.5	0.113	0.865	0.88	77 / 12
A. fasciculatum	28	4.5	0.4	0.092	1.063	0.84	235 / 26
A. fasciculatum	7	1.6	0.4	0.071	1.051	0.91	100 / 5
Q. berberidifolia	68	8.8	0.6	0.112	1.121	0.93	65 / 33
Q. berberidifolia	28	7.0	0.4	0.097	1.130	0.97	99 / 10
A. glandulosa	28	9.6	0.9	0.066	1.136	0.92	34 / 5
C. perplexans	28	5.5	1.1	0.097	1.037	0.82	35 / 19
C. perplexans	7	4.0	0.4	0.099	1.173	0.90	110 / 13
pooled	68	8.8	0.5	0.105	1.073	0.91	142 / 45
pooled	28	7.0	0.4	0.092	1.104	0.91	369 / 55
pooled	7	4.0	0.4	0.088	1.167	0.90	210 / 18

Dead biomass

species	stand burn age	max diameter (cm)	min diameter (cm)	$B_0*e^{0.5s}$	B_1	R^2	stems / shrubs
A. fasciculatum	68	2.30	0.7	0.047	1.249	0.65	14 / 4
A. fasciculatum	28	3.80	0.5	0.054	1.050	0.76	99 / 21
Q. berberidifolia	68	7.55	0.6	0.052	1.223	0.95	14 / 10
Q. berberidifolia	28	4.30	0.9	0.081	0.677	0.89	9 / 6
A. glandulosa	28/68	6.00	0.9	0.028	1.364	0.93	12 / 2
C. perplexans	28	3.25	0.7	0.052	1.166	0.96	16 / 7
charred stems	7	6.85	1.0	0.062	0.835	0.69	29 / 14
pooled	68	7.55	0.6	0.048	1.252	0.87	28 / 14
pooled	28	4.30	0.5	0.055	1.044	0.80	124 / 34
pooled	7	6.85	0.5	0.062	0.835	0.69	31 / 16

Table 2: Biomass measurements per plot. Charred stem biomass values are included for reference, but were not included in the total biomass values.

plot ID	plot age	Plot coordinates, latitude, longitude	plot area, m^2	live and dead biomass, kg	live and dead biomass, kg/m^2	Af, kg (% dead)	Ag, kg (% dead)	Qb, kg (% dead)	Cp, kg (% dead)	other broadleaf, kg (% dead)	subshrub, kg (% dead)	entirely dead shrub, kg	charred stems, kg
A	68	32.7990, -116.4532	63	386	6.1	5 (7%)	-	358 (2%)	-	15 (10%)	-	8	-
B	68	32.7988, -116.4531	57	221	3.9	113 (12%)	28 (1%)	66 (6%)	-	5 (43%)	-	9	-
C	68	32.7993, -116.4532	53	224	4.2	-	-	172 (11%)	-	1 (7%)	13 (17%)	38	-
D	68	32.7988, -116.4526	58	209	3.6	179 (18%)	5 (6%)	20 (8%)	-	2 (8%)	-	3	-
E	68	32.7992, -116.4528	45	337	7.5	-	10 (1%)	227 (6%)	-	41 (5%)	-	59	5
F	28	32.8024, -116.4545	61	209	3.4	98 (13%)	4 (0%)	35 (5%)	62 (7%)	1 (15%)	-	9	12
G	28	32.8026, -116.4540	54	280	5.2	1 (8%)	19 (3%)	167 (6%)	6 (18%)	15 (24%)	1 (46%)	71	4
H	28	32.8020, -116.4539	51	182	3.6	106 (20%)	1 (0%)	18 (8%)	27 (6%)	11 (3%)	4 (53%)	15	4
I	28	32.8024, -116.4539	55	222	4.0	113 (13%)	27 (9%)	22 (5%)	17 (11%)	17 (13%)	11 (22%)	15	16
J	28	32.8021, -116.4539	44	197	4.5	21 (4%)	-	84 (8%)	54 (15%)	17 (8%)	1 (2%)	20	7
K	7	32.7989, -116.4412	56	66	1.2	48 (12%)	-	-	10 (26%)	-	5 (4%)	3	63
L	7	32.8009, -116.4407	56	81	1.4	51 (1%)	-	-	28 (0%)	1 (3%)	1 (0%)	-	33
M	7	32.8006, -116.4406	54	71	1.3	48 (1%)	5 (1%)	-	17 (0%)	-	1 (0%)	-	43
N	7	32.8007, -116.4406	50	81	1.6	42 (0%)	21 (4%)	5 (0%)	5 (0%)	8 (1%)	-	-	44
O	7	32.8008, -116.4405	70	74	1.1	26 (0%)	-	10 (3%)	28 (0%)	7 (0%)	2 (8%)	1	22

I calculated percent dead material as the total biomass of entirely dead stems (attached to live shrubs) relative to the total (live and dead) shrub biomass for a given species. It varies substantially, but is generally higher in *A. fasciculatum* than other species, and overall much lower in the 7-year-old area. Since partially dead stems were categorized as "live" if green leaves were still present, these values represent the lower bound of percent dead biomass. Biomass from entirely dead shrubs is also highly variable and almost completely absent in the 7-year-old area.

Since I cannot make statistical inferences regarding the overall stand composition based on the field data due to the sampling technique (I selected plots that represented the range of variability found in the study area rather than random plots), I instead present general observations about the species composition and overall biomass present in the field plots. For this reason I do not present averages or estimates of error associated with plot biomass values.

The image classification product of species groups was assessed to have an overall accuracy of 71% (Table 3), based on reference data from the 1 m x 1 m field-based validation sample plots. Accuracy was higher in the more abundant categories of broadleaf and narrowleaf, and particularly low in the dead biomass category. An example of the classification results is shown in Figure 4.

Table 3: Error matrix from field-based accuracy assessment of the classified high spatial resolution map

		Field classification						
Remote Sensing Classification		Narrow-leaf	Bare	Broadleaf	Dead	Subshrub	Total	User's accuracy
	Narrowleaf	10	1	4	0	0	15	0.67
	Bare	0	2	0	0	1	3	0.67
	Broadleaf	3	0	17	2	0	22	0.77
	Dead	1	0	0	0	0	1	0.00
	Subshrub	0	0	0	0	1	1	1.00
	Total	14	3	21	2	2	42	
	Producer's accuracy	0.71	0.67	0.81	0.00	0.50		Overall accuracy 0.71

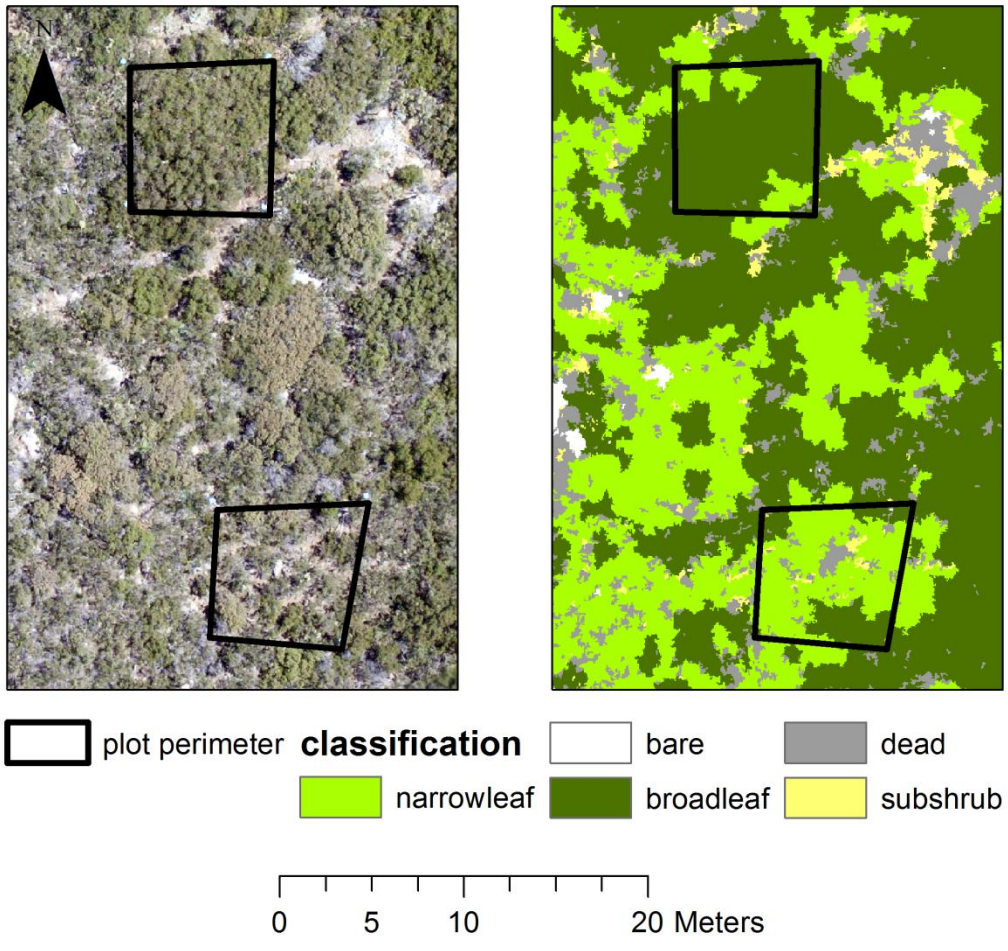

Figure 4: Example of classification results for two field plots within the 68-year-old stand.

Estimated biomass per area ranges from 6.2 kg m^{-2} in the oldest age class of broadleaf vegetation to 0.4 kg m^{-2} in the youngest age class of subshrub vegetation (Table 4). There were not enough areas of subshrub in the 68-year-old plots to calculate an average, so the values for these plots were estimated from the 28-year-old plots. Dead biomass per area values fluctuate so widely that it is not possible to calculate realistic values with the procedure used for the rest of the species groups. I simply use a value of 2 kg m^{-2} to approximate dead vegetation. This approximation is based on half the value calculated for the combined 68- and 28-year-old narrowleaf coefficient. The biomass per area coefficients provide a good approximation of the two major categories of shrub species (narrowleaf and broadleaf) and of overall biomass (Figure 5a-c). The predicted narrowleaf biomass values based on the mapped cover tend to yield a closer agreement with the field-measured plot biomass values, while the broadleaf and the combined total calculations are more variable.

Table 4: Above-ground biomass per unit area based on classification

veg type	age class	kg m^{-2}
broadleaf	68	6.2
broadleaf	28	4.2
broadleaf	7	2.4
broadleaf	68/28	5.2
narrowleaf	68	4.3
narrowleaf	28	3.6
narrowleaf	7	1.4
narrowleaf	68/28	4
subshrub	68/28	1.5
subshrub	7	0.4

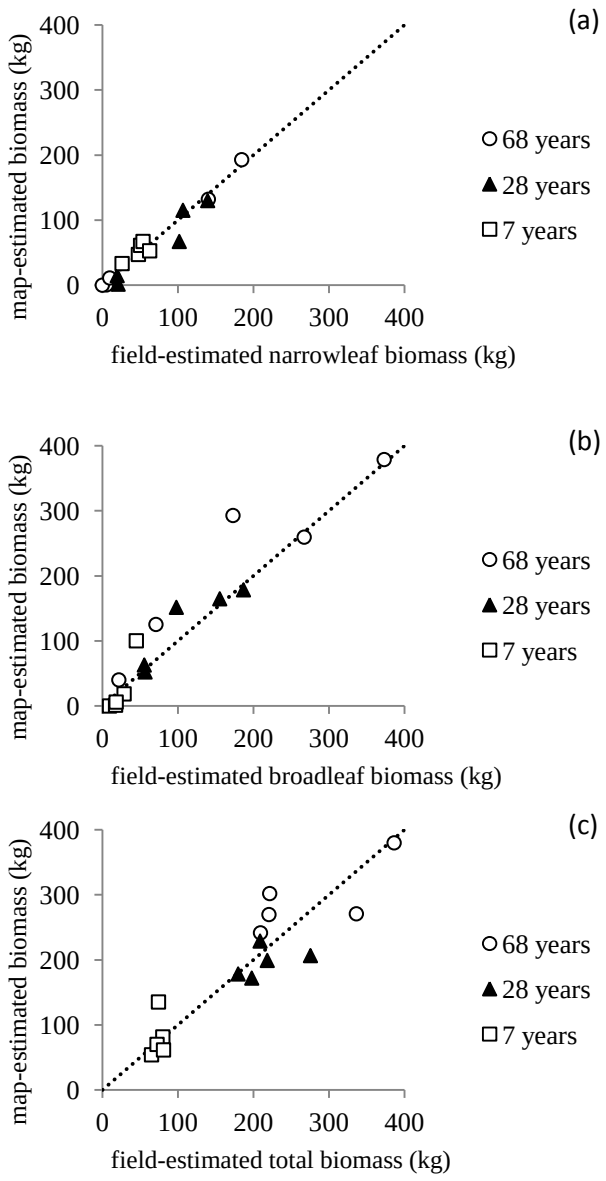

Figure 5: Field-estimated biomass vs biomass estimated using age-specific biomass coefficients in each field plot for a) narrowleaf, b) broadleaf, and c) total biomass. The dotted line is the 1:1 line.

There is a significant difference in mean biomass in the three age classes when using age-specific biomass coefficients ($F_{2,87} = 326$, $p < 0.001$), and the post-hoc Tukey test reveals that all three means are significantly different (Table 5, Figure 6). The calculated biomass values show a clear trend of accumulation through time (Figure 6). However, the differences between age classes are not as clear when using the biomass values calculated using pooled

coefficients (average of 28- and 68-year-old areas). Although the overall ANOVA is significant ($F_{2,87} = 243$, $p<0.001$), the post-hoc Tukey test reveals that the 28- and 68-year-old areas are not significantly different (Table 5, Figure 6). An overall trend of increasing biomass through time is evident, but when using these pooled coefficients, the difference between the 68- and 28-year-old areas is not significant (Figure 6). Both the results from the age-specific and pooled coefficients reveal a wide range in biomass values for each stand age calculated for the 30 sampling plots (Table 5).

Table 5: Mean, range, and ANOVA results for stand-level biomass comparisons using age-specific and pooled biomass coefficients. Df = 2,87, *n* = 30

	7 years	28 years	68 years	F	p
age-specific mean (kg/m^2)	1.3	3.4	5.1	326	<0.001
range	0.5 to 2.2	1.6 to 4.0	3.8 to 6.0		
pooled mean (kg/m^2)	1.3	4.0	4.4	243	<0.001
range	0.5 to 2.2	1.9 to 4.9	3.5 to 5.1		

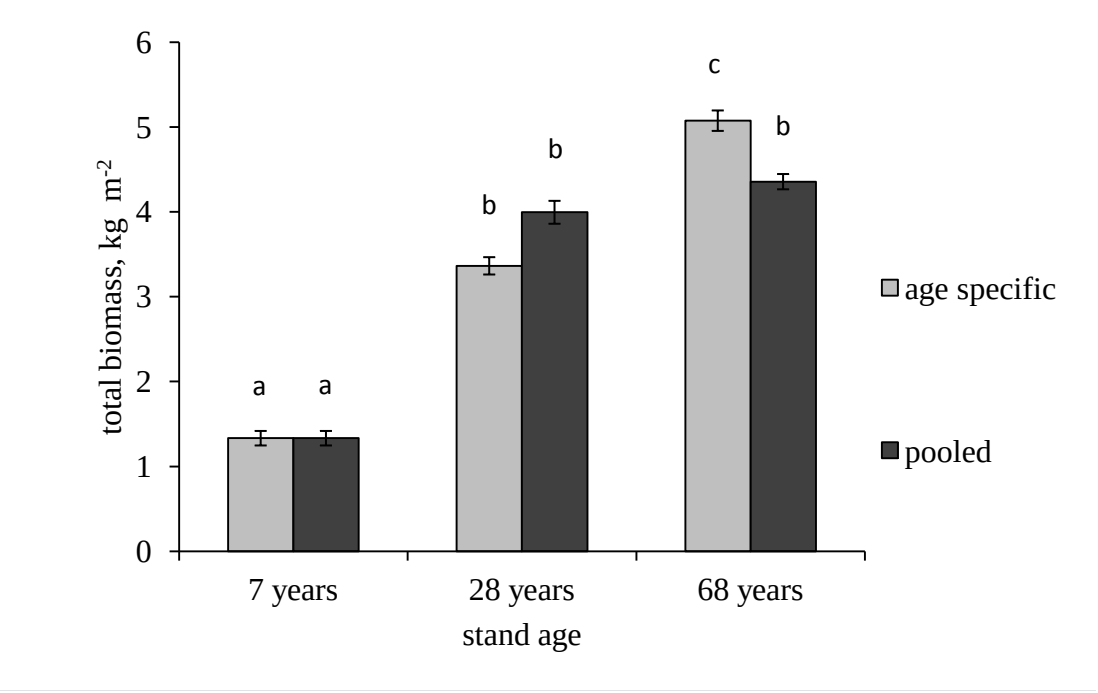

Figure 6: Total biomass means using a) age-specific biomass coefficients and b) pooled biomass coefficients. Error bars indicate standard error and letters indicate post-hoc Tukey tests. Bars with different letters are significantly different (p<0.05)

2. Landscape properties

The general trend of average percent cover in the 60 m x 60 m study areas within each burn area indicates that broadleaf percent cover is higher in the older areas, subshrub cover is lower, and bare is not different (Figure 7). Narrowleaf cover is greater in the 28- than 7-year-old area, and is similar in the 28- and 68-year-old areas. However, closer inspection of the associated ANOVA results indicates that while there is a significant cover difference among several of the vegetation classes in each age class (for example, broadleaf, $F_{2,15}$ = 10.2, p = 0.0016), post-hoc Tukey tests reveal that only the youngest age class is significantly different from the two older age classes (Table 6, Figure 8a). The post-hoc Tukey tests shows the same pattern for the narrowleaf category, and in the subshrub category, only the youngest and oldest age classes are significantly different (Figure 8a).

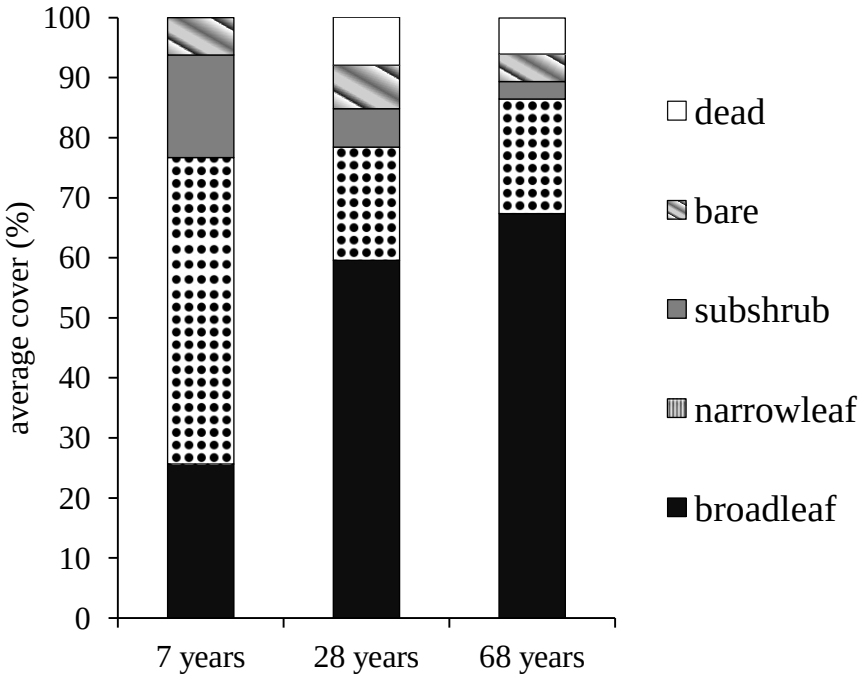

Figure 7: Average percent cover in the three age classes. Note that dead cover could not be estimated in the 7-year-old age class.

In general across stand ages, the aggregation index (landscape pattern metric) is higher (more aggregated) in the broadleaf and narrowleaf classes, and lower (more dispersed) for the subshrub and bare categories. Within the three age classes, only in the narrowleaf and subshrub categories are there significant differences in aggregation index with age (narrowleaf $F_{2,15} = 6.8$, $p = 0.0079$, subshrub $F_{2,15} = 6.9$, $p = 0.0077$)(Table 6). Post-hoc Tukey tests show that in the narrowleaf category, only the 7- and 28-year-old age classes are significantly different from one another, and in the subshrub category, only the 7- and 68-year-old age classes are significantly different (Figure 8b).

Area-weighted patch mean area is greater for the older age classes in the broadleaf category, with only the difference between the youngest and oldest age class being

significant ($F_{2,15}$ = 8.0, p = 0.0042) (Table 6). Patch mean area was lower in the youngest age class in the narrowleaf category, and the youngest area is significantly different than the two older areas ($F_{2,15}$ =15.8, p = 0.0002) (Figure 8c).

Table 6: ANOVA results for class and landscape metrics for the classified standardized resolution (0.5 m) dataset. Bold p-value indicates significant results ($p \leq 0.01$). Df = 2,15, n = 6

class	metric	mean 7 years old	mean 28 years old	mean 68 years old	F	p
broadleaf	aggregation	83	86	89	3.0	0.0816
narrowleaf	aggregation	81	65	70	6.8	**0.0079**
subshrub	aggregation	53	39	31	6.9	**0.0077**
bare	aggregation	44	63	53	3.8	0.0477
broadleaf	% of landscape	26	60	67	10.2	**0.0016**
narrowleaf	% of landscape	51	19	19	13.9	**0.0004**
subshrub	% of landscape	17	6	3	6.7	**0.0083**
bare	% of landscape	6	7	5	0.9	0.4315
broadleaf	mean patch area (m^2)	321	1514	2155	8.0	**0.0042**
narrowleaf	mean patch area (m^2)	1293	173	127	15.8	**0.0002**
subshrub	mean patch area (m^2)	79	5	3	4.1	0.0378
bare	mean patch area (m^2)	6	20	10	1.8	0.2059

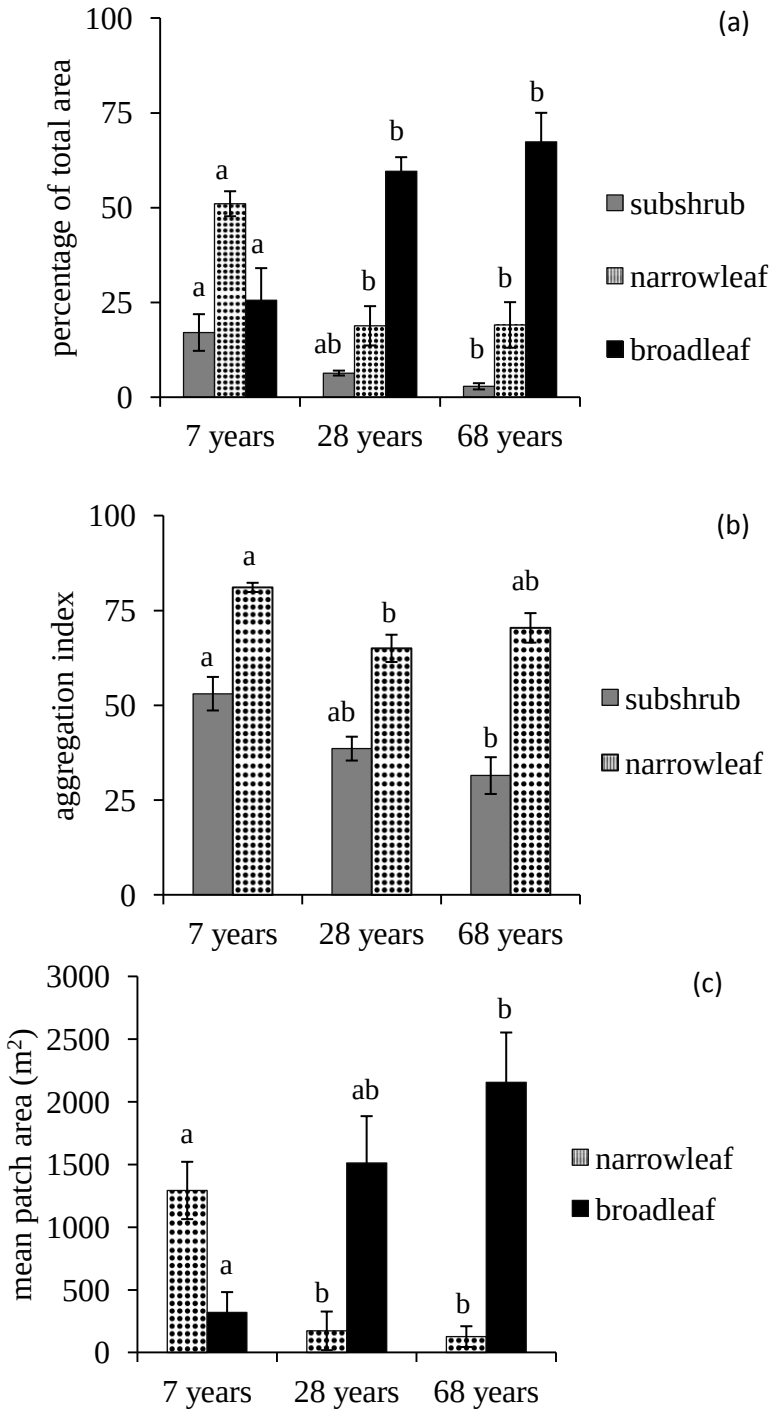

Figure 8a-c: Mean and standard error of significantly different age classes for the: a) percentage of total area for subshrub, narrowleaf and broadleaf categories, b) aggregation index for narrowleaf and broadleaf categories, and c) mean patch area for narrowleaf and broadleaf categories from the standardized resolution (0.5 m) dataset. Letters indicate post-hoc Tukey comparisons. Bars with different letters are significantly different ($p \leq 0.05$).

In addition to the ANOVA results for the landscape metrics from the classified standardized resolution (50 cm) images of the three age classes, I also performed a series of t-tests on the landscape metrics from only the higher resolution (4 cm) classified imagery from the two older age classes.

The only cover classification/ landscape metric combination that is significantly different in the two ages is percent cover of subshrub, which is higher for the 28-year-old area (df = 9.561, p = 0.009) (Table 7).

Table 7: T-test results from comparison of landscape metrics for classification of original resolution (4 cm) imagery from 68 and 28 year-old sites. Bold p-value indicates significant results ($p \leq 0.01$). $n = 6$

class	metric	mean 28 years old	mean 68 years old	df	p
broadleaf	aggregation	98	99	6.091	0.419
narrowleaf	aggregation	95	96	10.000	0.266
subshrub	aggregation	88	87	9.505	0.697
bare	aggregation	95	93	6.670	0.182
dead	aggregation	88	89	9.992	0.935
broadleaf	% of landscape	60	68	7.255	0.389
narrowleaf	% of landscape	19	19	9.783	0.982
subshrub	% of landscape	6	3	9.561	**0.009**
bare	% of landscape	7	5	9.930	0.084
dead	% of landscape	8	6	9.108	0.228
broadleaf	mean patch area (m^2)	1477	2105	9.850	0.269
narrowleaf	mean patch area (m^2)	168	147	8.814	0.910
subshrub	mean patch area (m^2)	4	5	6.338	0.922
bare	mean patch area (m^2)	19	10	7.250	0.297
dead	mean patch area (m^2)	3	3	9.848	0.852

E. Discussion and Conclusion

1. Stand-level biomass

There is a high degree of variability in biomass in the study area due to species composition and stand age. Although I was unable to perform a rigorous statistical analysis on this portion of the data due to sampling constraints, the general patterns observed seem reasonable. Older stands have higher levels of biomass per area, and coefficients of the tall, dense species that make up the broadleaf category are highest, followed by the more sparse narrowleaf category species, and finally by the much smaller subshrub species category. The regression equations calculated in this study are similar to those calculated in a previous study of the same area for the corresponding species and age (Riggan et al. 1988). The resulting biomass per area values are higher for each age than found by Riggan and others (1988), but similar to those found in other studies within southern California (Black 1987; Riggan et al. 1988). Although the exact biomass per area coefficient values are not necessarily applicable to areas outside of this field site, these values provide valuable field data to more accurately map and estimate stand-level biomass across the study area. Field-based biomass sampling is often too time consuming and logistically difficult to be conducted over large study areas (Lu 2006). Using remotely sensed imagery allows for biomass estimation over of much larger areas in an efficient manner. This approach of using high spatial resolution imagery with object-based methods is reasonably successful for mapping fine-scale variation in species composition. Considering all the potential sources of error and uncertainty due to geolocation accuracy, field measurement error, and other possible sources, it is promising that coefficients based on just two plots per stand age and species category yield such close agreement between field-estimated and map-estimated

biomass. Mapping success at the species category level (and by extension, biomass) could likely be further improved by using high spatial resolution color infrared imagery with object-based methods.

It is more challenging to derive reliable maps of dead biomass based on image-based classification. This is partly due to the tendency of dead biomass to be located beneath plant canopies composed mostly of live biomass, either as dead stems within a single shrub or as an entirely dead shrub surrounded by live shrubs. This means that although dead biomass is often spread uniformly throughout stands of chaparral, it is only occasionally visible from above (which would allow it to be measured through aerial imagery). These small patches of dead biomass are not representative of the total dead biomass found in an area and make it more difficult to derive a relationship for biomass per unit area.

I calculated stand-level biomass in two ways: once with age-specific coefficients, then again with coefficients for the pooled data from the 28- and 68-year-old sites. As explained earlier, I did this to provide a more cautious estimate of biomass in the 28- and 68-year-old sites due to the small sample size from which the coefficients were calculated. While results for the age-specific coefficients show a substantially higher biomass for the 68-year-old areas, the results from the pooled coefficients indicate that the difference is not significant. It is possible that if the 68-year-old area had substantially more broadleaf cover than the 28-year-old area, the broadleaf coefficient (higher than the narrowleaf coefficient in both the age-specific and pooled calculations) might have resulted in a higher biomass value in both calculations. However, the difference in broadleaf cover is not significant between the two older years. Regardless of whether biomass continues to accumulate, it is clear that biomass levels remain high in old stands of chaparral, consistent with the findings of previous studies

(Black 1987; Specht 1969). Unsurprisingly, there is a large difference in biomass between the 7- year-old and 28-year-old stands. Shrub growth is rapid during this early phase of post-fire recovery and shrubs quickly expand in both cover and stature (Keeley and Keeley 1981; Rundel and Parsons 1979). Although there are site differences between the 7-year-old stand and the older stand, the measurements of biomass per unit area for each species are based on areas in which each species is dominant.

Although it is still uncertain whether or not biomass continues to accumulate appreciably at older stand ages, the high number of plots sampled through the scaling approach reveals a wide range of biomass values within a single age class. It is noteworthy that biomass from an even-aged stand varies so widely at the plot level (8 m x 8 m). This fine-scale spatial variation is typically difficult to map and might be important in understanding fire behavior (Keane et al. 2001).

The scaling approach used in this study uses two separate relationships, which has advantages and disadvantages. The final biomass values depend on both the stem-to-biomass regression relationship and the field measured biomass-to-mapped cover category relationship. The benefit of this approach is that it allows for estimates over a much larger study area than could be adequately achieved using field sampling alone, but the challenge is that there is increased potential for error to propagate through the calculations. However, the high degree of fine-scale variation observed in this study indicates that it is likely worthwhile to expand the study area through this scaling approach at the cost of some degree of accuracy.

2. Landscape properties

Although landscape properties between the 28- and 68-year-old areas are not substantially different, several significantly different relations were identified between the 7-year-old site and the older sites. Broadleaf cover and patch size are larger, while narrowleaf cover and patch size are smaller in the older age classes. Subshrub cover is also lower in the older age classes. While some of these differences might be due to age, it is difficult to make definitive comparisons in landscape properties between the 7-year-old site and the two older sites due to the slightly different aspect of the younger stand (more southeast facing, compared to the more directly east facing older sites).

Another potential issue with these landscape-level comparisons is that the original classification of the youngest age site was based on a different (and lower resolution) imagery source than the older age classes. While I reduced the spatial resolution of the older age classes to make the results more comparable, it is possible that the results would be different had I been able to use high spatial resolution imagery for the entire study area. In particular, I likely would have been able to more accurately classify the small (but abundant) patches of bare area observed during field sampling in the youngest age class. However, the overall trends I observe through the analysis of image-derived landscape properties seem consistent with observations in the field.

It is also important that almost no significant differences in the landscape properties of the 28- and 68-year-old stands were identified, even when the high spatial resolution classification results were compared. Other than a small difference in subshrub cover, there are no differences in aggregation, percent of landscape, or patch size in these two older age classes. Although I was unable to confidently relate field measurements of dead biomass to

classified dead biomass cover, it is still noteworthy that there is no significant difference in the landscape-level properties of dead biomass in the two older age classes. A high level of dead biomass in the oldest stand could indicate age-related die back, as observed by Hanes (1971). However, I observe no such age-related shrub die back in the older age classes, consistent with the findings of Keeley (1992).

3. Summary

This study indicates that shrub biomass within the Kitchen Creek study area remains high in chaparral that is at least 68-years-old. While it is unclear whether there is a net accumulation in biomass from the age of 28 to 68, there is little difference in the spatial arrangement of species groups in the two age groups. Biomass per unit area for each species is much lower in the 7-year-old stand compared to the two older stands, and it seems reasonable to expect that for a given species, the trend towards higher biomass with increasing age reflects the process of post-fire shrub recovery. Due to the difference in aspect in the youngest stand, it is more difficult to determine if the differences in total biomass and landscape properties represent an age-related trend. In all age classes, I found a wide range of biomass values, indicating a high degree of spatial variability within chaparral.

Although the field sampling was somewhat limited due to the physically difficult and time consuming nature of the measurements in barely penetrable mature chaparral shrublands, I was able to extend the study area through the use of high spatial resolution imagery and OBIA classification of vegetation types. This approach of combining detailed field measurements with remotely sensed classification of species types provides insight on

fine-scale patterns of species distribution and biomass, which could be related to fire behavior.

Chapter 3: Chaparral growth ring analysis as an indicator of stand biomass development

A. Abstract

Wildfires in chaparral typically create even-aged stands that grow quickly in the first two decades following a fire. While patterns of biomass accumulation are important for understanding ecosystem productivity, it is often logistically challenging to measure growth over long time periods. In this study, I tested the utility of a novel method of using shrub growth rings to estimate stand-level biomass accumulation at an annual time scale in southern California chaparral. I examined how temporal variation in precipitation and spatial variation in flow accumulation and solar irradiation levels influence those biomass accumulation patterns. Using field measurements and the relationship between stem basal area and total biomass, I estimated current biomass levels in an 11-year-old chaparral stand, and used growth rings diameters to estimate growth in each year from 4- to 11-years-old. I examined the relationship between annual growth and annual precipitation, and found that annual growth tracks closely with patterns of annual precipitation. Solar irradiation and flow accumulation at each plot was also calculated to explore relationships related to energy and water balance, but were not significant covariates with total biomass. Growth ring analysis is a promising technique for estimating several years of post-fire growth using a single season of field work.

B. Introduction

Wildfires are a common occurrence in chaparral ecosystems, and typically consume nearly all above-ground biomass. Patterns of biomass accumulation are important for

understanding ecosystem productivity following a fire, which is closely related to the fuel available for future fires and their ecological fire effects (Riggan et al. 1988). Productivity in chaparral is often measured in the field for a limited number of years (for example, Black 1987; Pasquini and Vourlitis 2010; Schlesinger and Gill 1980) or using satellite-based vegetation metrics for a time span of up to a decade (Hope et al. 2007; Kinoshita and Hogue 2011), but tracking productivity in the field over a decade is logistically challenging. In addition to the difficulty of revisiting a site over such a long time period, chaparral vegetation is very dense and becomes nearly impassible to humans after only a few years of post-fire growth. In this study, I test a method for measuring stand-level biomass accumulation at an annual time scale using shrub growth rings, and examine how temporal variation in precipitation and site-specific factors co-vary with those biomass accumulation patterns.

Chaparral shrubs grow following a fire by resprouting from underground burls (obligate resprouters), by germinating from seeds (obligate seeders), or by a combination of resprouting and seed germination (facultative seeders). These obligate seeders typically germinate in the first year following a fire, and are very sensitive to seasonal water availability due to their shallow roots. In contrast, resprouting species can continuously resprout in the years following a fire, and are less sensitive to seasonal water availability due to the presence of established roots (Saruwatari and Davis 1989).

The sensitivity of obligate seeders to seasonal water availability and tendency to germinate only in the first year following a fire means that species with this post-fire strategy produce annual growth rings that can be interpreted relatively easily compared to resprouting species (Keeley 1993). Growth rings result from the contrast between lighter

colored wood formed during periods of rapid growth, and darker colored wood formed during periods of slower growth. Riggan and others (1988) have established regression relationships between shrub basal diameter and total shrub biomass in chaparral. Older shrubs might be more likely to have problems with heart rot, which makes the youngest rings impossible to interpret (Keeley 1993). With the assumption that the diameter of each growth ring corresponds to the diameter of the shrub at the end of that growing season, obligate seeder species provide an opportunity to measure annual increases in shrub biomass during the early post-fire recovery period.

Both the approach and resulting information on post-fire shrub growth at an annual scale represent unique contributions in the area of chaparral research. While previous studies have used chaparral growth rings to determine stand or shrub age (Duren and Muir 2010; Keeley 1993; Stohlgren et al. 1984; Zammit and Zedler 1993), shrub response to precipitation (Coale et al. 2011), and biomass accumulation at a seven year scale (Riggan et al. 1988), research relating growth rings to biomass at an annual scale is more common for (non-chaparral) trees (e.g. Bouriaud et al. 2005; Clark et al. 2001). Previous studies of post-fire recovery that follow a single stand through time have typically been limited to the first three (Pasquini and Vourlitis 2010) or four (Keeley and Keeley 1981) years of growth.

The selection of the specific southern California field site for this study (described below) was based on several important factors. The entire site predominantly consists of chaparral and burned in 2002, so the growth rings represent the early years of post-fire recovery. The area is dominated by obligate seeder species, which tend to produce easily interpretable growth rings. While resprouting species also do produce annual rings, I decided to start with the group of species that previous research had indicated would offer

the greatest chance of successful growth ring identification. In addition, previous research conducted at the site provides important reference information. In Riggan and others, (1988) biomass accumulation was estimated for stands within this site at 7- and 14-years-old using growth ring reconstruction in 21-year-old plots. The relationship between stem basal area and biomass was also determined here for a range of chaparral species and ages as part of this previous study.

The following research questions are addressed within the context of improving methods for quantifying biomass accumulation and understanding patterns of post-fire biomass accumulation: 1) Do measurements of shrub growth ring change increments provide a useful metric of biomass accumulation? 2) How does biomass accumulation of recovering shrubs, measured as the change in growth ring diameter, vary with differences in annual precipitation? How does this response vary with time-since-fire? 3) How do spatial patterns of shrub biomass accumulation vary with factors related to site energy and water balance (solar irradiation and flow accumulation)?

C. Methods

1. Study site

The San Dimas Experimental Forest (SDEF) is a research site managed by the US Forest Service located in the San Gabriel Mountains in Los Angeles County, CA, USA. It is predominantly covered by mixed chaparral vegetation, with coastal sage scrub, oak woodland, and mixed conifers also present. The obligate seeding species *Ceanothus crassifolius* is common on south facing slopes, and *Ceanothus oliganthus*, another obligate seeder, is common on north-facing slopes. *Quercus berberidifolia*, an obligate resprouter, is

also found occasionally on north-facing slopes and *Adenostoma fasciculatum*, a facultative seeder, is found in low abundance throughout SDEF. The entire study site burned in September of 2002. This area experiences a Mediterranean-type climate, with hot, dry summers and cool, wet winters. Average precipitation for the area is approximately 720 mm (http://www.prism.oregonstate.edu/, accessed 4 April 2014).

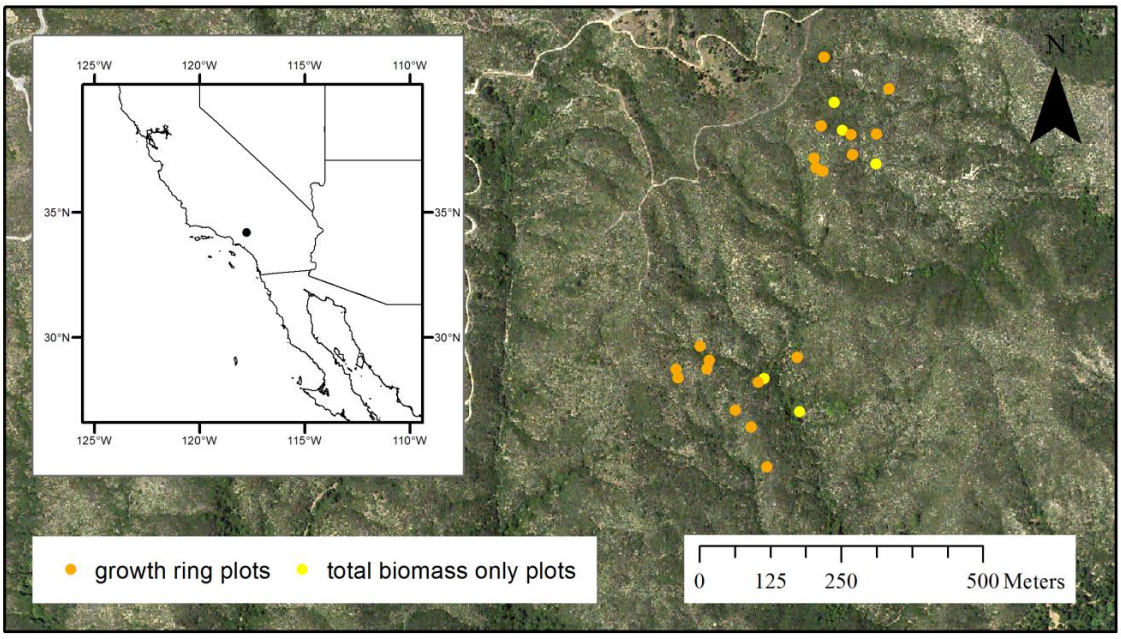

Figure 9: Location of San Dimas Experimental Forest (SDEF) and individual plot locations. Total biomass was measured at all 24 field plots, and growth rings were successfully processed at 19 of the plots. Background imagery is from the National Agricultural Imagery Program, acquired in 2012.

2. Field methods

Field plots are located within two 6.25 ha areas (250 m by 250 m) within 500 m of one another and were selected using the following criteria: 1) vegetation composed entirely of chaparral (no portion of the area classified as coastal sage scrub or coast live oak) and 2) reasonably accessible (within 100 m of a road or trail). Access was an important consideration because chaparral vegetation is usually very dense and difficult to traverse. I

established three randomly located replicate plots, each 16 m^2 (4 m x 4 m), stratified by aspect (north, south, east, west), in each of the two 6.25 ha study areas. This resulted in 12 plots per study area and a total of 24 for the entire site. All plot sampling took place in the autumn of 2013.

Plot boundaries were surveyed in the field using Trimble GeoXM handheld Global Positioning System (GPS) unit with a post-processed accuracy of 1 to 3 m. I measured all stems 0.4 cm or greater in diameter within the plots at 10 cm above the ground using digital calipers and recorded the species and if stems were live, dead, or charred. For irregularly shaped stems, I recorded the maximum and minimum stem diameters to determine the average stem diameter. Shrubs that were partially outside the plot were measured and included in plot estimates if more than half the stem area at the base was within the plot. Live stems were identified by the presence of green leaves. Stems that were mostly dead were still counted as live if green leaves were present. Stems were recorded from each shrub separately.

The biomass of each plot at the year of field sampling was calculated using species-specific regression equations relating stem basal area to dry biomass. I calculated coefficients for the relationship of dry above-ground biomass (*AGB*) as a power function of basal area (*BA*) with a bias correction applied (Baskerville 1972; Sprugel 1983):

$$\boldsymbol{AGB = B_0(BA)^{B_1}e^{0.5\,s}} \quad \text{Equation 2}$$

where *s* is the residual mean square, B_0 is the proportionality coefficient, and B_1 is the scaling exponent.

These regression equations were based on stems sampled during the 2013 field campaign and during an earlier field campaign in the autumn of 2011. I generated species-specific equations for *Adenostoma fasciculatum, Ceanothus crassifolius, Ceanothus oliganthus, Eriodictyon trichocalyx,* and *Q. berberidifolia*. I combined the measurements from each species sampled in more than one year to create a single regression equation for each species. I also used the regression equation for *Salvia mellifera* developed by Riggan and others (1988), and a regression equation calculated using all pooled stem measurements to calculate to biomass of any other species found in the field plots. Regression models were run separately for live and dead stems. Charred stems were only occasionally found in the plots, and were not the main focus of the study, so charred biomass was estimated in these areas using half the value given by the appropriate equation for dead biomass.

One shrub per species per day was selected to serve as a representative sample to estimate dry weight for the regression equations. Shrub water content varies seasonally (Countryman and Philpot 1970), and different species have different water-use patterns (Davis and Mooney 1986), so selecting one shrub per species per day provided an approximation for the water content of all shrubs of that species on a given day. Water content of shrubs of a given species likely also varies with shrub size, but this is a limitation of the sampling method I decided to accept in order to reduce the extensive field effort. A sampled shrub was brought to the lab where it was separated into small (< 0.5 cm), medium (0.5 cm to 2 cm) and large (>2 cm) diameter fractions. Each size fraction was weighed and subsampled to determine water content. Shrub components were dried to a constant mass in a drying oven at 100˚C. The total shrub water content was determined by applying the water

content value measured for each size fraction to the total biomass of each corresponding size fraction. This value was then applied to all shrubs of that species sampled on that day.

A species-specific equation was used to calculate shrub biomass for an average of 88% (and a per-plot range of 43 - 100 %) of the total basal area present in each plot. Although the number of both individual stems and shrubs from which those stems were harvested are presented, the regression relationships are based only on the basal area measurements of individual stems. The stems measured in the study plots were occasionally larger than the stems sampled destructively to calculate regression equations. Across all plots, an average of 2% of stems (and a per-plot range of 0 – 14%) were so large as to require an extrapolation of the regression equation to estimate biomass.

4. Growth ring processing

Stem cross sections from five randomly selected *Ceanothus spp.* (*C. crassifolius* and *C. oliganthus*) shrubs from each study plot were harvested in the field at a height of 10 cm using loppers (or a pruning saw for larger diameter stems). When a shrub had more than one stem present at 10 cm, the five largest stems were collected, although ultimately I only used the largest stem from each shrub for the growth ring analysis. The stem cross sections were sanded with progressively finer sandpaper up to 400 grit and photographed using a flat platform and stationary camera. I then measured the growth ring diameters along the maximum and minimum axis of each cross section using ImageJ software (Abràmoff et al. 2004).

I calculated the basal area for each year of growth using the mean of the maximum and minimum diameter measurements. Each year of growth was then converted to a percentage

of the total area (representing growth at the end of 2013), and the mean percent increment in basal area was calculated for each plot. I assumed that the bark width was a constant ratio of the total stem diameter (Bush and Brand 2008), and therefore used the inside bark measurements to calculate the percent increment values.

I applied the average plot-level percent increment to all live stems measured in each plot to estimate basal areas for each year of post-fire growth. The annual plot-level biomass values were then calculated for each year post-fire using these estimated basal area values and the species-specific regression equations described earlier. I did not attempt to calculate dead stems because it was difficult to determine which year each stem had died. Although dendrochronological studies typically use standardized growth ring widths to account for the decline in ring width age (Fritts and Swetnam 1989), in this study I used total area values because I related stem area directly to plot-level biomass increment.

5. Site-specific analysis

I calculated annual solar irradiation for each plot in order to explore spatial patterns related to energy and water balance. Sites with low irradiation levels are typically more mesic than sites with high irradiation due to lower evapotranspiration rates (Roder et al. 2008), with lower biomass typically associated with sites with higher irradiation (Yool et al. 1985). I calculated the annual irradiation at the center of each plot using a lidar-based digital elevation model (DEM) resampled to 1 m as input into the hemispherical viewshed algorithm implemented in ArcGIS software (Rich et al. 1994). I also used the DEM to calculate the actual slope aspect of each plot, as slight errors in plot placement sometimes resulted in plots that did not match the planned aspect. I then grouped the plots into three

categories based on aspect: northeast – northwest, southeast to southwest, and directly east or west facing.

In addition, I calculated the average Normalized Difference Vegetation Index (NDVI) for each plot using color infrared (CIR) imagery with a spatial resolution of 1 m. The imagery was collected in May 2012 as part of the National Agriculture Imagery Program (NAIP). NDVI was calculated as the difference of uncalibrated digital number values for the average near infrared and average red wavebands divided by the sum of those values for each plot. Examining the average plot NDVI allowed me to compare another metric of vegetation abundance (independent of the field-measured biomass) with the annual solar irradiation. This served as a verification of the patterns I observed with the field-measured biomass.

In order to further investigate spatial patterns related to water availability, I calculated the mean flow accumulation values (i.e., number of upslope DEM cells that connect to a given cell) for each plot using a 0.5 m DEM and ArcGIS software. In this analysis, the number of upslope contributing cells is determined for each grid cell. I then calculated the average upslope contributing area for each plot.

6. Data analysis

I examined the relationship between annual precipitation, year-since-fire, and average annual biomass growth by calculating the Pearsons's product correlation coefficient (r) for each pair of variables (n = 7). I examined the correlation rather than regression for this exploratory analysis because the time-series dataset does not meet the criteria of independence necessary for a regression model. Precipitation data were obtained from the

PRISM climate group (http://www.prism.oregonstate.edu/, accessed 4 April 2014) and summed by water year (12 month period starting Oct 1st of each year, designated by the calendar year in which it ends). The PRISM (Parameter-elevation Regressions on Independent Slopes Model) interpolation method uses physiographic factors to weight weather station observations (Daly et al. 2008).

For the site-specific analysis, I performed several linear regression analyses: total biomass and irradiation (n = 24), total biomass and NDVI (n = 24), NDVI and irradiation (n = 24), and total biomass and flow accumulation (n = 24). I examined the coefficient of determination (R^2) for each regression. All statistical analyses were conducted using the R statistical software package.

D. Results

1. Plot biomass

Regression models of biomass as a function of basal area for the five chaparral species are presented in Figure 10, and regression coefficients are shown in Table 8. The R^2 values for the biomass equations are high and range from 0.79 to 0.98. The R^2 values for dead biomass are lower and range from 0.29 to 0.89 (Table 9).

The average biomass of live shrubs at the time of field sampling (11-years-old) was 2.6 kg m^{-2}, with a range of 1.0 – 6.7 kg m^{-2} (Table 10). This estimation includes dead biomass attached to living shrubs. Entirely dead shrubs were found on many of the plots, as were charred stems. *C. crassifolius* occurred in high abundance on most plots, and *A. fasciculatum* and *S. mellifera* were also commonly present. *Ceanothus oliganthus*, *Eriodictyon trichocalyx*, *Quercus berberidifolia*, *Eriogonum fasciculatum*, *Cercocarpus betuloides*,

Heteromeles arbutifolia, and *Prunus ilicifolia* were also occasionally found. The two plots with the highest biomass are north-facing plots dominated by *C. oliganthus* and *Q. berberidifolia*, which are species commonly associated with north-facing slopes (Dunn et al. 1988; Keeley 2000). However, not all north-facing plots have high levels of biomass, or even species associated with north-facing slopes. A small quantity of entirely dead shrubs were observed within many of the plots, and the biomass of dead material on live shrubs typically made up less than 5% of total biomass, although it was occasionally as high as 10%.

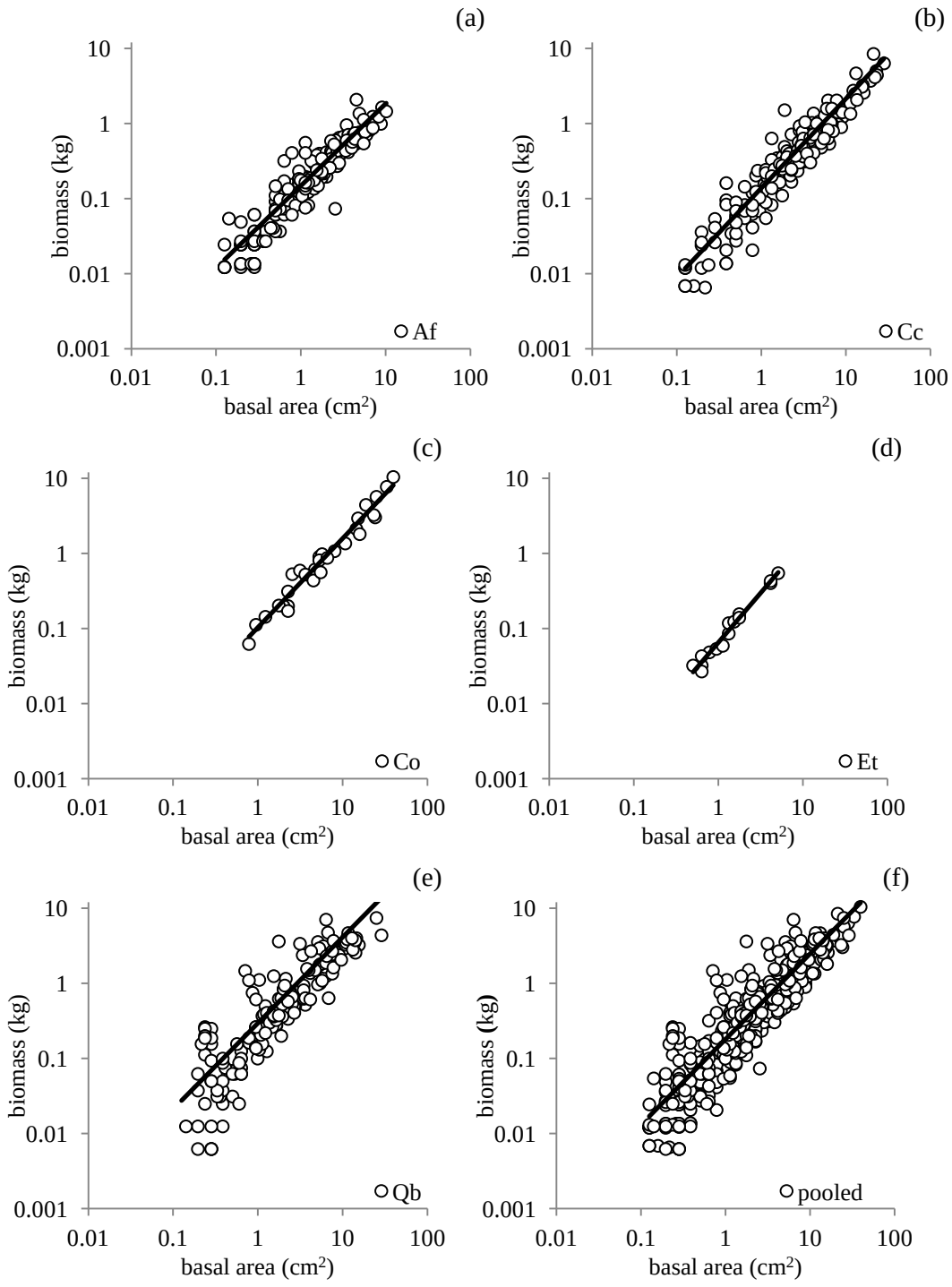

Figure 10: Scatter plots and least squares regression lines for biomass as a function of basal area for a) *Adenostoma fasciculatum,* b) *Ceanothus crassifolius,* c) *Ceanothus oliganthus,* d) *Eriodictyon trichocalyx* e) *Quercus berberidifolia* and f) all pooled measurements, which was used for the small number of species which lacked a species-specific regression equation

Table 8: Regression coefficients of stem biomass (kg) as a function of basal area (cm^2) for live stems. The pooled coefficients were calculated by combining measurements across all species.

species	max diameter (cm)	min diameter (cm)	$B_0 * e^{0.5s}$	B_1	R^2	stems / shrubs
A. fasciculatum	3.6	0.4	0.148	1.093	0.89	197/13
C. crassifolius	6.0	0.4	0.138	1.188	0.91	182/62
C. oliganthus	7.1	1.0	0.103	1.185	0.96	30/16
E. trichocalyx	2.6	0.8	0.065	1.319	0.98	15/11
Q. berberidifolia	6.1	0.4	0.296	1.144	0.79	167/6
pooled	7.1	0.4	0.179	1.136	0.84	591/108

Table 9: Regression coefficients of stem biomass (kg) as a function of basal area (cm^2) for dead stems. The pooled coefficients were calculated by combining measurements across all species.

species	max diameter (cm)	min diameter (cm)	$B_0 * e^{0.5s}$	B_1	R^2	stems / shrubs
A. fasciculatum	1.05	0.5	0.053	0.5	0.29	8/3
C. crassifolius	1.95	0.5	0.079	1.184	0.89	13/6
Q. berberidifolia	1.9	0.4	0.226	1.037	0.52	33/4
pooled	1.95	0.4	0.163	1.093	0.55	54/13

Table 10: Biomass measurements per plot. Total shrub biomass calculations include dead stems attached to otherwise live shrubs. The percent of this dead stem biomass relative to total biomass is presented for each species total. Plots listed in italics had insufficient stem cross section samples and were not included in biomass per year estimations. Species listed include *Ceanothus crassifolius* (*Cc*), *Adenostoma fasciculatum* (*Af*), *Salvia mellifera* (*Sm*), *Ceanothus oliganthus* (*Co*), *Eriodictyon trichocalyx* (*Et*), *Quercus berberidifolia* (*Qb*), *Eriogonum fasciculatum* (*Ef*), *Cercocarpus betuloides* (*Cb*), *Heteromeles arbutifolia* (*Ha*), *Prunus ilicifolia* (*Pi*).

		Biomass (kg m^{-2})											
plot ID	aspect	combined total live shrub (includes attached dead)	entirely dead shrubs	charred stem estimate	*Cc* total shrub biomass (% dead)	*Af* total shrub biomass (% dead)	*Sm* total shrub biomass (% dead)	*Et* total shrub biomass (% dead)	*Co* total shrub biomass (% dead)	*Qb* total shrub biomass (% dead)	other total shrub biomass (% dead)	other species	total stems
plot 1	East	1.1	-	-	0.9 (<1%)	-	-	-	-	-	0.1 (0%)	*Ef*	39
plot 2	South	2.3	0.1	-	1.1 (0%)	-	-	0.7 (4%)	-	-	0.3 (3%)	*Ef*	150
plot 3	East	2.0	0.5	0.1	0.7 (<1%)	0.6 (0%)	-	0.1 (3%)	-	-	-		201
plot 4	North	1.1	0.2	0.1	0.3 (0%)	-	-	-	0.2 (0%)	-	0.4 (0%)	*Cb*	54
plot 5	Southwest	1.0	-	-	0.6 (<1%)	-	0.4 (0%)	-	-	-	0.1 (0%)	*Ef*	83
plot 6	West	2.4	0.4	-	0.2 (0%)	0.3 (2%)	1.5 (0%)	-	-	-	-		246
plot 7	Northeast	1.6	0.1	-	1.1 (<1%)	0.4 (<1%)	-	-	-	-	-		172
plot 8	Southwest	2.5	0.2	-	1.7 (<1%)	-	0.6 (5%)	-	-	-	-		99
plot 9	South	2.4	0.3	0.1	1 (0%)	-	0.1 (0%)	-	-	-	0.9 (9%)	*Ef*	281
plot 10	Southwest	1.8	-	0.3	0.1 (3%)	1.1 (<1%)	0.5 (0%)	-	-	-	-		160
plot 11	Northeast	2.4	0.1	0.5	1.8 (0%)	0.3 (0%)	-	0.2 (9%)	-	-	-		105
plot 12	East	1.7	0.3	-	0.6 (0%)	-	0.2 (0%)	-	-	-	0.5 (0%)	*Ef*	78
plot 13	Southwest	1.7	-	0.4	0.8 (0%)	0.6 (2%)	0.2 (0%)	-	-	-	-		153
plot 14	Northeast	3.4	-	0.1	1.8 (0%)	-	-	-	-	-	1.5 (0%)	*Ha*	96
plot 15	East	2.3	0.1	0.4	2.2 (0%)	-	-	-	-	-	-		119
plot 16	East	1.2	0.1	0.6	0.6 (<1%)	0.5 (1%)	-	-	-	-	-		63
plot 17	South	3.9	0.3	0.9	2.1 (1%)	1.5 (4%)	-	-	-	-	-		205
plot 18	Northeast	2.9	0.2	-	2.7 (4%)	-	-	-	-	-	-		323
plot 19	Northeast	4.7	0.6	1.0	-	-	-	-	3 (0%)	1.1 (0%)	-		80
plot 20	Northeast	6.7	-	2.1	0.1 (0%)	-	-	-	2.6 (2%)	4 (10%)	-		110
plot 21	Southwest	2.5	0.2	-	2.3 (<1%)	-	-	0.1 (2%)	-	-	-		152
plot 22	Southwest	2.9	-	-	1.2 (0%)	-	0.5 (0%)	1.2 (3%)	-	-	-		105
plot 23	South	4.4	0.6	-	-	-	-	-	3.8 (3%)	-	-		100
plot 24	West	4.4	-	0.6	1.1 (<1%)	-	-	-	-	-	3.3 (<1%)	*Pi, Cb*	106
mean		2.6	0.2	0.3									
sd		1.4	0.2	0.5									

2. Growth rings

Of the 24 field plots, five were removed from analysis because there were fewer than three stem cross sections per plot of suitable quality (Table 10). I found that it was difficult to clearly determine ring position in stems smaller than approximately 1 cm. Shrubs were sampled randomly in the field, which sometimes resulted in the collection of several small stems from a single plot. In addition, some shrubs had heart rot or insect damage, which obscured the center rings, and in other shrubs, the smallest center rings were difficult to differentiate. In order to make use of the stems that lacked rings from the earliest years of post-fire recovery while maintaining a consistent number of measurements per year in each plot, I started the analysis at the fourth year of post-fire recovery (the 2005 – 2006 growing season).

The percent of total stem area in each year is shown for each of the final 19 plots in Figure 11a. The difference between each year of growth is shown in Figure 11b. Most plots show a peak that occurs at year nine (the growth that occurred during the 2010-2011 growing season). This pattern persists when the differences in area are converted to differences in biomass, as shown in Figure 12a - c. Although many of the plots appear to have a less pronounced peak when viewed in terms of biomass increment compared to percent area increment, this is simply due to the smaller range in values in low-biomass plots. The biomass increment peak at year nine is aligned with the year of highest precipitation during the study period (Figure 12d). A positive and significant correlation is found between annual precipitation and average annual biomass growth ($r = 0.75$, $p = 0.05$, $n = 7$). The correlation between year-since-fire and average annual biomass growth is not significant ($r = 0.48$, $p = 0.3$, $n = 7$).

Figure 13 compares the range of biomass values found in this study for the plots in which growth rings were available and *C. crassifolius* was dominant (15 total) with the range of values previously measured using a 21-year-old growth ring reconstruction of 11 *C. crassifolius* dominated plots (Riggan et al. 1988). The two datasets show very similar growth trajectories for the overlapping time period.

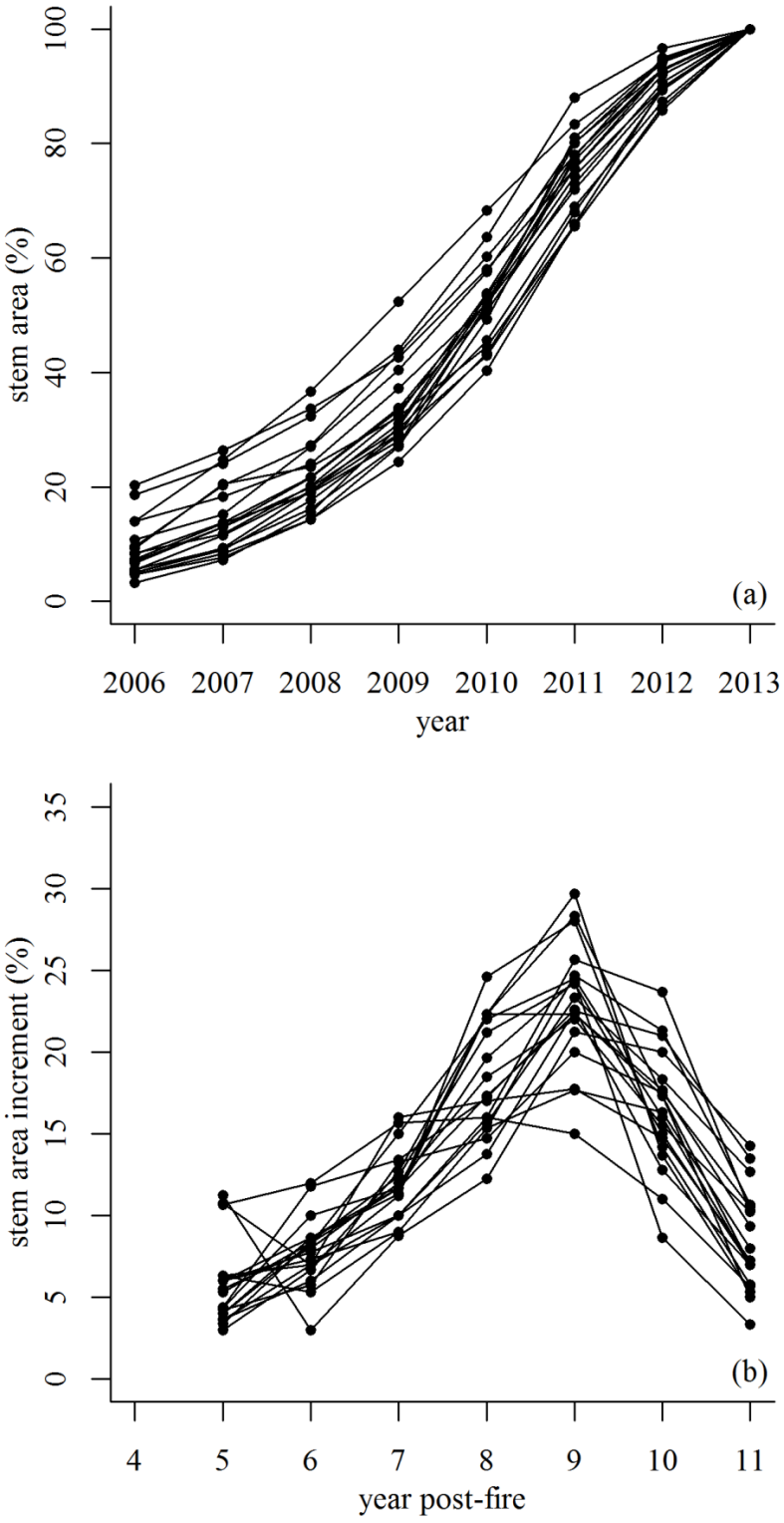

Figure 11: a) Per-plot annual percent of total stem area for the 19 plots in which sufficient growth ring samples were collected. The calendar year represents the growth that has occurred by the fall of that year. b) annual stem area increment plotted as year since last fire (occurred in 2002).

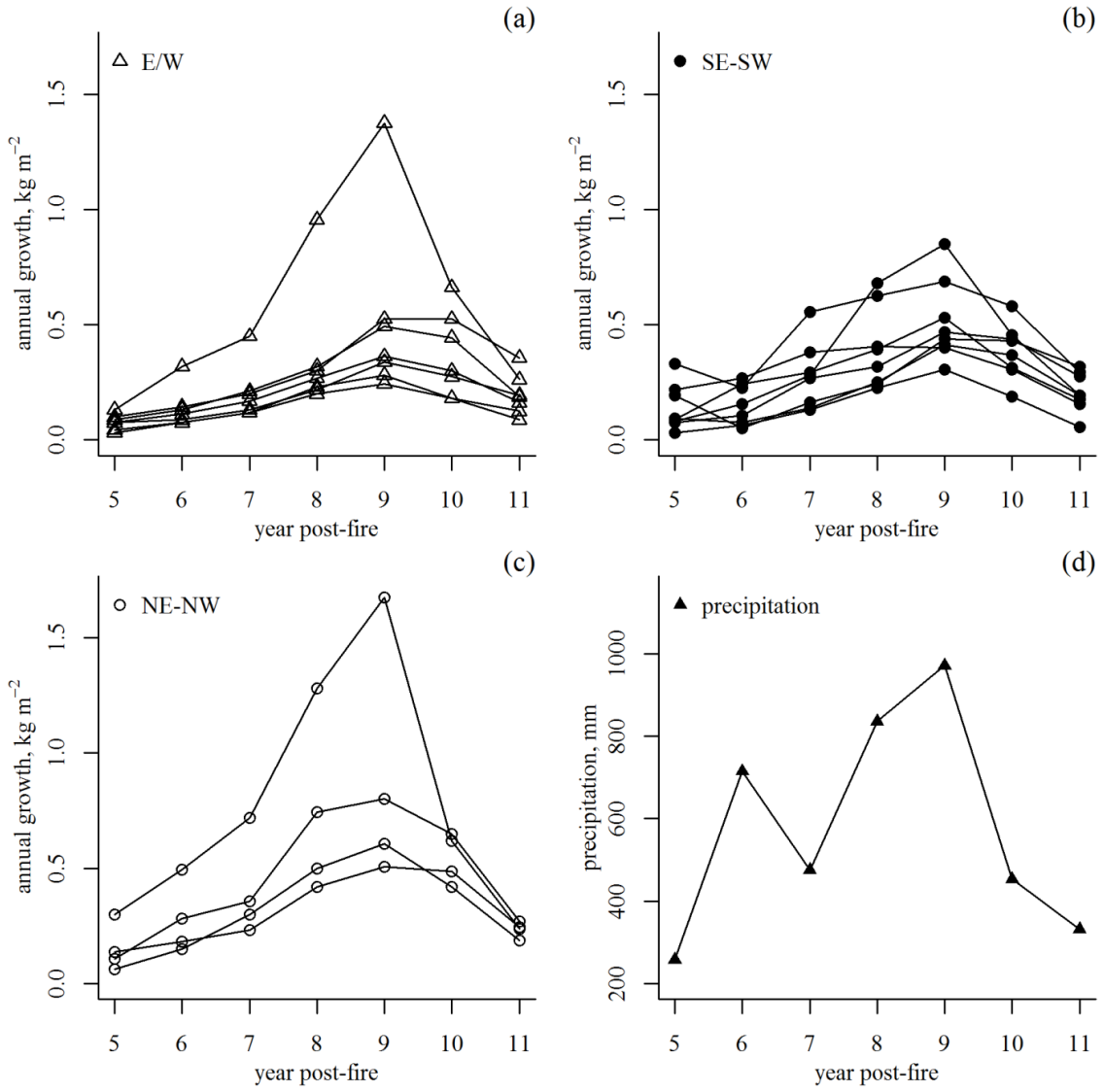

Figure 12: Annual biomass increment in each year post-fire in plots facing (a) directly east or directly west, (b) southeast to southwest, and (c) northeast to northwest. Annual precipitation is shown in (d).

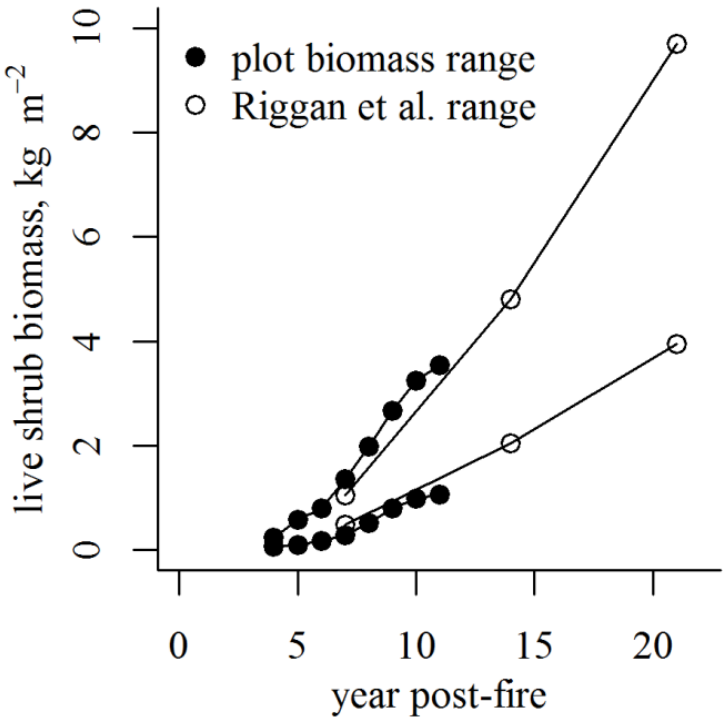

Figure 13: Maximum and minimum annual biomass values in *C. crassifolius* dominated plots from this study (years 4 through 11 post-fire) and values reconstructed from growth ring measurements of 21-year-old *C. crassifolius* plots from the same general study area in Riggan et al. 1988 (years 7,14, and 21 post-fire).

3. Site-specific analysis

I performed the irradiation analysis to assess whether patterns of shrub biomass are associated with energy and water balance. This analysis requires only the final biomass values, so I included the full set of 24 plots. While the irradiation values match the plot aspect (north-facing plots have lower irradiation values than south-facing plots), low irradiation plots do not have corresponding high biomass (Figure 14a). The regression of annual irradiation and total plot biomass is not significant ($R^2 = 0.02$, $p = 0.5$, n = 24).

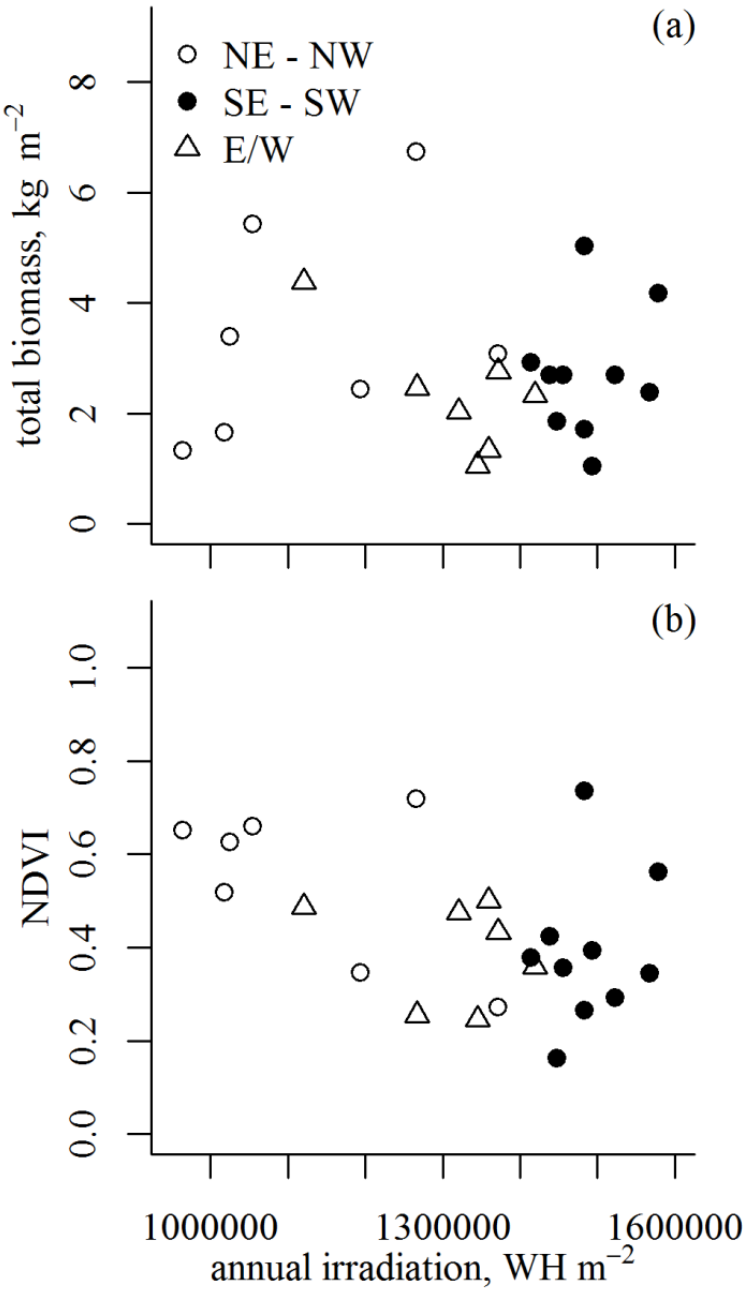

Figure 14: a) Total biomass and annual irradiation in watt hours per square meter for each of the 24 field plots b) NDVI and annual irradiation. Plots are grouped into categories of northeast to northwest, southeast to southwest, and directly west or east facing.

I calculated the average plot NDVI to serve as an independent verification of the pattern of irradiation and vegetation abundance. The regression of annual irradiation and NDVI is not highly significant (R^2 = 0.20, p = 0.03, n = 24, Figure 14b). However, the regression of total biomass and NDVI is significant (R^2 = 0.37, p = 0.002, n = 24, Figure 15).

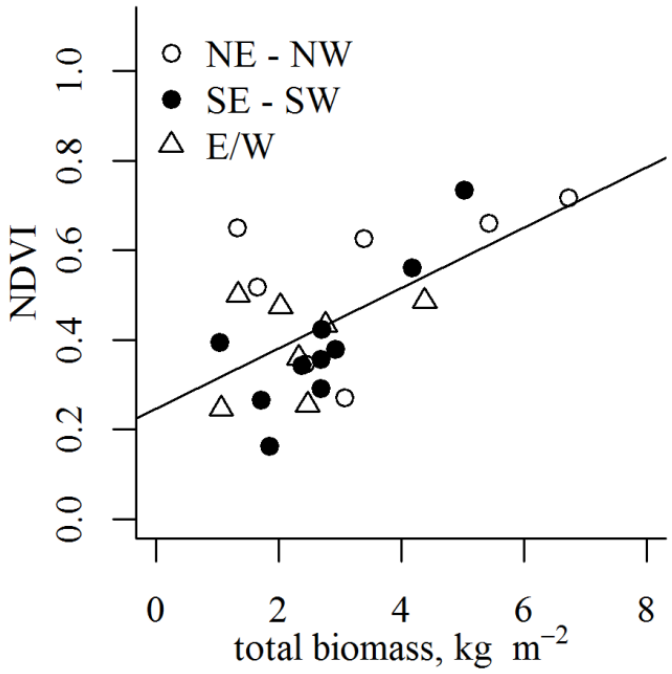

Figure 15: Total biomass and NDVI for the 24 field plots.

I calculated the flow accumulation values to serve as a metric of water availability. There is no significant relationship between total biomass and upslope contributing area (R^2 = 0.02, p = 0.5, n = 24, Figure 16).

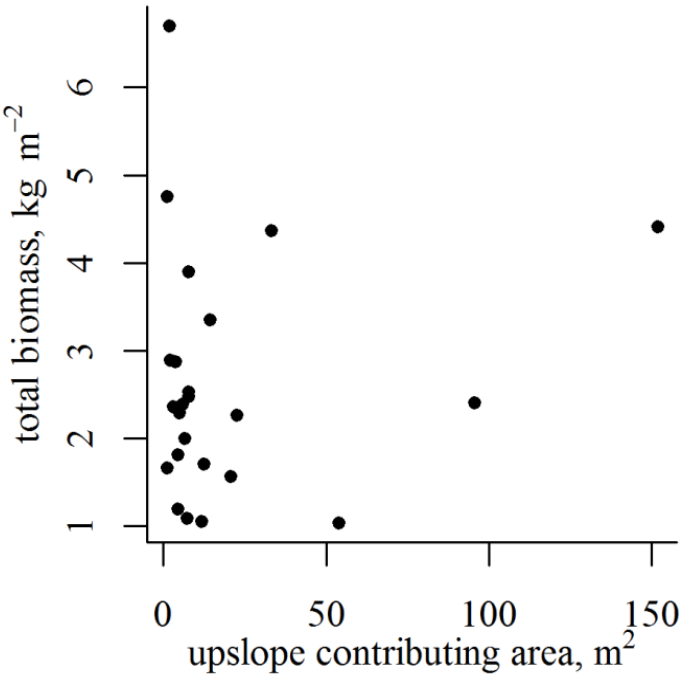

Figure 16: Flow accumulation analysis, showing upslope contributing area and total biomass for the 24 field plots.

E. Discussion and Conclusion

In this study, I explored the extent to which shrub growth rings and growth ring increments provide useful metrics of shrub biomass and accumulation, and examined the ways that annual biomass accumulation varies with precipitation and time-since-fire. I also tested the relationship between the spatial pattern of biomass recovery and site-specific factors of solar irradiation and flow accumulation.

1. Growth rings

I found that shrub growth rings provide a relatively straightforward and valuable method to track patterns of biomass accumulation in the early years of post-fire recovery. Field work in general (and particularly in chaparral) is labor-intensive and logistically challenging. This approach provides the ability to estimate several years of growth using only a single season

of field sampling. Although additional research would be useful to quantify the relationship between plot biomass estimated using this technique and plot biomass measured during the actual year of growth, the results of this study indicate that this is a promising technique.

While most plots show a consistent overall temporal pattern of growth that tracked with the temporal variation of annual precipitation, there is considerable variation among plots, particularly when calculated as annual biomass growth (Figure 12). This indicates that multiple plots within a stand are necessary to adequately characterize the overall mean biomass accumulation and/or pattern of stand development. Previous studies indicate that precipitation plays an important role in shaping the patterns of post-fire recovery (Hope et al. 2007) and that the pattern of recovery is spatially variable (Kinoshita and Hogue 2011). This study supports these observations, and provides additional detail about how biomass recovery varies on an annual basis.

Although annual plot growth does not show a significant relationship with stand age, this is likely due to the short duration of the study, the influence of annual precipitation variation, and a likely non-linear relationship between growth and age. Previous studies indicate that the rate of growth in chaparral declines with time after the first two decades of recovery (Black 1987; Rundel and Parsons 1979). A longer sequence of ages would be necessary to understand the relationship between biomass accumulation, precipitation, and stand age. Growth rates appear to decline in the last two years of the study, but this is likely due to two years of low precipitation, rather than due to stand age. This lack of statistical relationship of growth rate with stand age for the time period measured is supported by the reference 21-year-old recovery sequence shown in Figure 13 (Riggan et al. 1988). The range of biomass values from the same study area, measured in 1981, matches the range found in

this study remarkably well, and indicates that biomass is likely to continue to sharply increase over the next decade.

While it is useful to convert the stem cross sectional area to biomass, it requires the assumption that the regression equation relating biomass to stem area is consistent across years. Riggan and others (1988) indicate that the regression equation is significantly different in 7- and 14-year-old stands of chaparral because of the rapid growth that occurs during the early stages of stand development. Since these equations specify higher biomass per stem area for the older age stands, using equations to calculate biomass for younger stands will likely result in an overestimation of biomass. However, obtaining equations for each year of the early post-fire years would require substantial additional field work, and it would have needed to start immediately after the 2002 fire. I decided that for the purposes of this project, it is reasonable to accept some small amount of overestimation of biomass in the younger ages.

Ceanothus crassifolius and *oliganthus* shrubs produce rings usable for this analysis of early post-fire recovery, but due to issues with heart rot and insect damage after just a few years, tracking growth over a long time period using cross sections collected at a single point in time might be more difficult. It might be possible to track longer periods of growth by revisiting a developing stand multiple times, several years apart.

2. Site-specific analysis

I examined annual solar irradiation as a covariate of biomass after 11 years of growth because it is an important factor in the energy and water balance, and I expected it to be closely related to total biomass. This was not the case in this study, and it is not clear why no relationship was observed. Species associated with north-facing slopes were more common

on plots of that aspect, but overall, species composition did not show a clear association with solar irradiation or aspect. Irradiation has been shown in other studies of Mediterranean-type landscapes to be a useful predictor of biomass (Dahlin et al. 2012; Yool et al. 1985), and of green vegetation cover (Roder et al. 2008). The flow accumulation analysis also did not reveal any relationship between water availability and biomass. Most plots had a relatively small upslope contributing area. It is possible that if more plots with larger upslope contributing areas were included, a more meaningful pattern would be revealed.

One possible explanation for the lack of statistical relationship with biomass is that there could be co-location errors and uncertainty between plot locations and the DEM from which irradiance and accumulated flow estimates are derived. However, NDVI also shows little relationship with irradiation, and this is not dependent on any sort of field-based error. NDVI does exhibit a realistic relationship with measured biomass.

There are several possible explanations for the lack of agreement in biomass and terrain related variables. The spatial extent of the study area and number of plots might both be too small to detect a relationship. The fine spatial resolution of the DEM might actually be causing more confusion if small facets are masking the overall energy and water balance pattern. Differences in soil properties could also be partially responsible for some of the biomass patterns. Although the entire study area is mapped as being a single soil type, the soils likely vary in their water retention capabilities, possibly influencing plant available moisture. Differences in species composition patterns could also be partially masking the relationship.

Another possible factor related to the lack of agreement in biomass and terrain-related variables might be that the study area is still in the early stages of post-fire recovery, and was not yet at a state of full canopy closure. Shrubs become dominant and return to pre-fire cover levels within ten to fifteen years following a fire (Keeley et al. 1981; McMichael et al. 2004), but biomass continues to increase with time (Riggan et al. 1988). Perhaps at a later stage of stand development, the biomass values would show more consistency with irradiation. As noted earlier, it appears from previous work in this area that biomass will continue to increase sharply in the next decade (Figure 13, Riggan et al. 1988). Low precipitation and the associated low rates of growth in the last two years of recovery could also be a factor in the lack of agreement in biomass and terrain-related variables.

Related to the problem of canopy closure is the issue of plot size. I choose to use 4 x 4 m plots because the smaller area was more tractable than the 8 x 8 m plot size I had used in a previous chaparral study (Uyeda et al. in review) especially considering the large number of plots. However, it is possible that plots 16 m^2 in area do not fully capture the variability found in the study area, particularly if the canopy closure process is incomplete.

The use of shrub growth rings is a promising technique for reconstructing the stand development patterns of early post-fire chaparral. For the time period I examined, precipitation has a significant role in shaping the annual patterns of biomass growth, and time-since-fire was not a significant factor. Although I expected solar irradiation to have a significant role in determining spatial patterns of biomass accumulation through its control on evapotranspiration, I was not able to detect any meaningful patterns of co-variability. In future work, I plan to relate the biomass recovery patterns measured here to satellite-based metrics of vegetation growth. This will help to determine if such plot biomass to satellite

metric relationships provide a feasible way to scale field-intensive measures of shrub growth across larger extents.

Chapter 4: Combining ground-based measurements and MODIS-based spectral vegetation indices to track biomass accumulation in post-fire chaparral

A. Abstract

Multi-temporal satellite imagery can provide valuable information on patterns of vegetation growth over large spatial extents and long time periods, but corresponding ground-referenced biomass information is often difficult to acquire, especially at an annual scale. In this study, I test the relationship between annual biomass estimated using shrub growth rings and metrics of seasonal growth derived from Moderate Resolution Imaging Spectroradiometer (MODIS) spectral vegetation indices (SVIs) for a small area of southern California chaparral to evaluate the potential for mapping biomass at larger spatial extents. The site had most recently burned in 2002, and annual biomass accumulation measurements were available from years 5 – 11 post-fire. I tested metrics of seasonal growth using six SVIs (Normalized Difference Vegetation Index, Enhanced Vegetation Index, Soil Adjusted Vegetation Index, Normalized Difference Water Index, Normalized Difference Infrared Index 6, and Vegetation Atmospherically Resistant Index). While additional research would be required to determine which of these metrics and SVIs are most promising over larger spatial extents, several of the seasonal growth metrics/ SVI combinations have a very strong relationship with annual biomass, and all SVIs have a strong relationship with annual biomass for at least one of the seasonal growth metrics.

B. Introduction

Wildfires in chaparral commonly occur over vast expanses of land (Keane et al. 2008). Remotely sensed imagery provides a spatially comprehensive view of the post-fire recovery process, and recent studies have used multi-temporal imagery from sources such as Landsat Thematic Mapper / Enhanced Thematic Mapper Plus (Hope et al. 2007), Advanced Visible/Infrared Imaging Spectrometer (AVIRIS) (Riaño et al. 2002b), and Aqua/Terra Moderate Resolution Imaging Spectroradiometer (MODIS) (Kinoshita and Hogue 2011) to study post-fire recovery in chaparral. MODIS data in particular provide an excellent opportunity to study post-fire recovery because processed datasets are available with high temporal resolution (8 or 16 days, depending on the product) going back to 2000. Spectral vegetation index (SVI) products such as normalized difference vegetation index (NDVI) are generated from radiometrically calibrated, atmospherically corrected and geometrically processed MODIS data. The high temporal resolution allows researchers to study the properties of recovery throughout the entire growing season, rather than at just one or a few times of the year. Seasonal growth metrics based on the full SVI time-series provide detailed information about vegetation recovery (van Leeuwen et al. 2010).

The long record length of MODIS data allows for single stands to be tracked through time. Previously, studies of multi-temporal satellite image analyses of chaparral growth following fire have been based on chronosequence approaches to sampling SVI values (e.g., NDVI, NDVI-derived leaf area index and green vegetation fraction) across landscapes (Henry and Hope 1998; McMichael et al. 2004; Peterson and Stow 2003). In a chronosequence approach, space is substituted for time, such that SVI values are sampled from different age stands to create a SVI time trajectory. While this approach allows for

only one or a few well processed images to be used to generate trajectories, some shortcomings are that it does not account for variability related to precipitation (Uyeda et al. 2015) and might miss variability within single age stands, which can substantial (Uyeda et al. in review).

Although remote sensing studies provide valuable information on post-fire recovery, deriving accurate biomass measurements from remotely sensed data is difficult (Lu 2006), and many studies of post-fire recovery either don't include field data (Kinoshita and Hogue 2011), or provide only cover data (van Leeuwen et al. 2010). The lack of accurate biomass measurements is an important limitation in studying post-fire recovery (Uyeda et al. 2015).

Previous studies have found a strong correlation between tree ring width and estimates of net primary productivity based on NDVI data in boreal forests (Malmström et al. 1997) and with tree ring width and integrated NDVI in the central Great Plains (Wang et al. 2004). Annual changes in oak tree circumference measured over a ten year period were strongly correlated with integrated annual Enhanced Vegetation Index (EVI) (Garbulsky et al. 2013). These studies provide evidence of strong relationships between satellite-based measures of annual growth and field-based metrics in mature forested areas, although it is not yet known if strong relationships would also be found in post-fire shrublands.

In a previous study, I examined the relationship between shrub fractional cover measured using high spatial resolution color infrared imagery and MODIS NDVI for several chaparral stands in the first two decades of post-fire recovery (Uyeda et al. 2015). I found that tracking a single stand through time revealed important details on the recovery process compared to the chronosequence approach. However, an important limitation of the study

was the lack of field-measured biomass data. In another earlier work, I found that the use of shrub growth rings and regression equations relating shrub biomass to stem basal area can be an effective method for estimating biomass accumulation in the early years of post-fire chaparral recovery (Uyeda et al. in prep).

In this study, I expand on these earlier works to compare annual biomass accumulation measured using shrub growth rings with MODIS-based metrics of vegetation growth in a seven year post-fire recovery period in chaparral shrublands. I test several metrics of annual growth from multiple spectral vegetation indices to address the following research questions: 1) Which MODIS-based metrics of annual growth are most closely related to ground-based measurements of annual biomass accumulation in chaparral obligate seeder shrubs and what is the degree of temporal co-variability? 2) Is the relationship between MODIS-based growth metrics and biomass sufficiently strong to indicate a potential for mapping biomass growth at regional scales?

C. Methods

1. Study site

The San Dimas Experimental Forest (SDEF) is a research site managed by the US Forest Service located in the San Gabriel Mountains in Los Angeles County, CA, USA. It is predominantly covered by mixed chaparral vegetation, with coastal sage scrub, oak woodland, and mixed conifers also present. The obligate seeding species *Ceanothus crassifolius* is common on south facing slopes, and *Ceanothus oliganthus*, another obligate seeder, is common on north-facing slopes. *Quercus berberidifolia*, an obligate resprouter, is also found occasionally on north-facing slopes and *Adenostoma fasciculatum*, a facultative

seeder, is found in low abundance throughout SDEF. The entire study site burned in September of 2002. This area experiences a Mediterranean-type climate, with hot dry summers and cool wet winters. Average precipitation for the area is approximately 720 mm (http://www.prism.oregonstate.edu/, accessed 4 April 2014).

2. Field work

The full details of field sampling methods are provided in Uyeda et al. (in prep). Field plots are located within two 6.25 ha areas (250 m by 250 m) within 500 m of one another. I established three randomly located replicate plots, each 16 m^2 (4 m x 4 m), stratified by aspect (north, south, east, west), in each of the two 6.25 ha study areas. This resulted in 12 original plots per study area and a total of 24 for the entire site. However, five plots were later removed from the analysis, resulting in a final number of 9 plots in the northern study area and 10 in the southern study area (Figure 17). At each plot, I measured all stem diameters at the height of 4 cm and collected stem cross sections from five randomly selected *Ceanothus spp.* shrubs. All plot sampling took place in the autumn of 2013.

Species specific regression equations relating stem diameters to dry shrub biomass were calculated from destructive sampling of shrubs that took place during the autumn 2013 sampling, as well as from nearby sampling from autumn 2011. These shrubs have a close relationship between stem diameter and dry shrub biomass, with coefficient of determination (R^2) values ranging from 0.79 to 0.98 (Uyeda et al. in prep).

The stem cross sections were sanded with progressively finer sandpaper up to 400 grit and photographed using a flat platform and stationary camera. I then measured the growth

ring diameters along the maximum and minimum axis of each cross section using ImageJ software (Abràmoff et al. 2004).

I calculated the basal area for each year of growth using the mean of the maximum and minimum diameter measurements. Each year of growth was then converted to a percentage of the total area (representing growth at the end of 2013), and the mean percent increment in basal area was calculated for each plot. I assumed that the bark width was a constant ratio of the total stem diameter (Bush and Brand 2008), and therefore used the inside bark measurements to calculate the percent increment values. I applied the average plot-level percent increment to all live stems measured in each plot to estimate what the basal area would have been in each year. The annual plot-level biomass increment was then calculated for each year post-fire using the previously described regression equations. I then calculated the average of the annual growth increment for each of the two study areas. Due to problems with interpreting the smallest growth rings on some of the shrubs, I started the analysis at the fourth year of recovery. This means that annual change in biomass data is available for years 5 – 11 after the fire. Although dendrochronological studies typically use standardized growth ring widths to account for the decline in ring width age (Fritts and Swetnam 1989), in this study I used total area values because I related stem area directly to plot-level biomass increment.

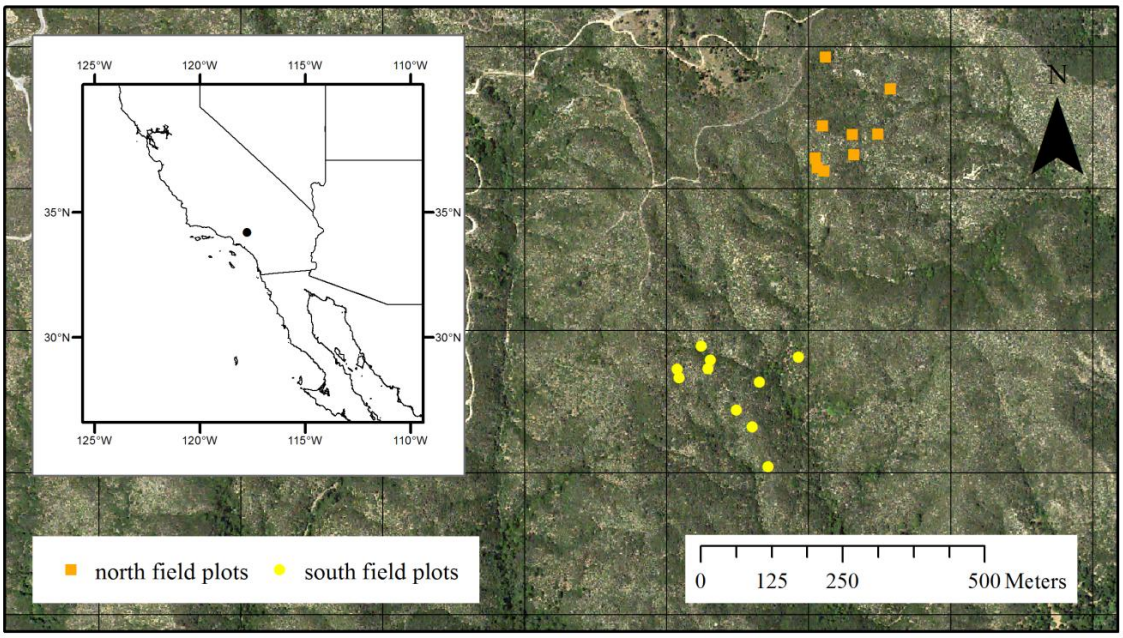

Figure 17: Field site in San Dimas Experimental Forest, Los Angeles County, California. Gridlines show the nominal MODIS MOD13Q1 footprint boundaries.

4. Image processing

MODIS MOD13Q1 vegetation index and MCD43A4 nadir bi-directional reflectance distribution function (BRDF) products for tile h08v05 were downloaded from the Land Processes Distributed Active Archive for dates starting February 2000 through 2013. All image datasets were reprojected from Sinusoidal to Universal Transverse Mercator projections, then subset to the study area. Using the MODIS vegetation index product (MOD13Q1), I created a time series of NDVI and EVI from February 2000 – December 2013 for the two pixels whose ground resolution elements encompass the study sites. The MOD13Q1 product is atmospherically corrected, has a spatial resolution of 250 m, and is produced using 16 day composite periods.

I also calculated spectral vegetation indices (SVIs) using the MODIS nadir bi-directional reflectance distribution function (BRDF) adjusted reflectance product (MCD43A4) for the

two pixels within the study sites. The MCD43A4 product has a spatial resolution of 500 m and is produced using 8 day composite period. The SVIs calculated from this product include NDVI, EVI, Soil Adjusted Vegetation Index (SAVI), Normalized Difference Water Index (NDWI), Normalized Difference Infrared Index 6 (NDII6), and Vegetation Atmospherically Resistant Index (VARI). Equations for each SVI are given in Table 11.

Table 11: Equations for each Spectral Vegetation Index. Subscripts correspond to MODIS band numbers (band 1 = 620 – 670 nm, band 2 = 841 – 876 nm, band 3 = 459 – 479 nm, band 4 = 545 – 565 nm, band 5 = 1230 - 1250 nm, band 6 = 1628 - 1652 nm)

Spectral Vegetation Index	equation	reference
NDVI	$\frac{\rho_2 - \rho_1}{\rho_2 + \rho_1}$	(Rouse et al. 1973)
EVI	$2.5 * \frac{\rho_2 - \rho_1}{\rho_2 + 6 * \rho_1 - 7.5 * \rho_3 + 1}$	(Huete et al. 2002)
SAVI	$\frac{\rho_2 - \rho_1}{\rho_2 + \rho_1 + 0.5} * (1 + 0.5)$	(Huete 1988)
NDWI	$\frac{\rho_2 - \rho_5}{\rho_2 + \rho_5}$	(Gao 1996)
NDII6	$\frac{\rho_2 - \rho_6}{\rho_2 + \rho_6}$	(Hunt and Rock 1989)
VARI	$\frac{\rho_4 - \rho_1}{\rho_4 + \rho_1 - \rho_3}$	(Gitelson et al. 2002)

All time series were smoothed using the Savitzky-Golay filtering algorithm and gap-filled to remove low-quality data using TIMESAT software (Jonsson and Eklundh 2004). For each of the seven growing seasons and each SVI (NDVI, EVI, SAVI, NDWI, NDII6, and VARI), I output several of the growth metrics calculated in TIMESAT. These metrics include the maximum (the highest smoothed value observed during the growing season),

base value (the average of the minimum values from the beginning and end of the growing season), amplitude (difference between the maximum and base value) and the small and large integral of the seasonal growth curve (small is the area between the growth curve and the base value, large is the total area below the growth curve) (Figure 18). In addition, I selected the un-smoothed SVI observed in mid-August of each year.

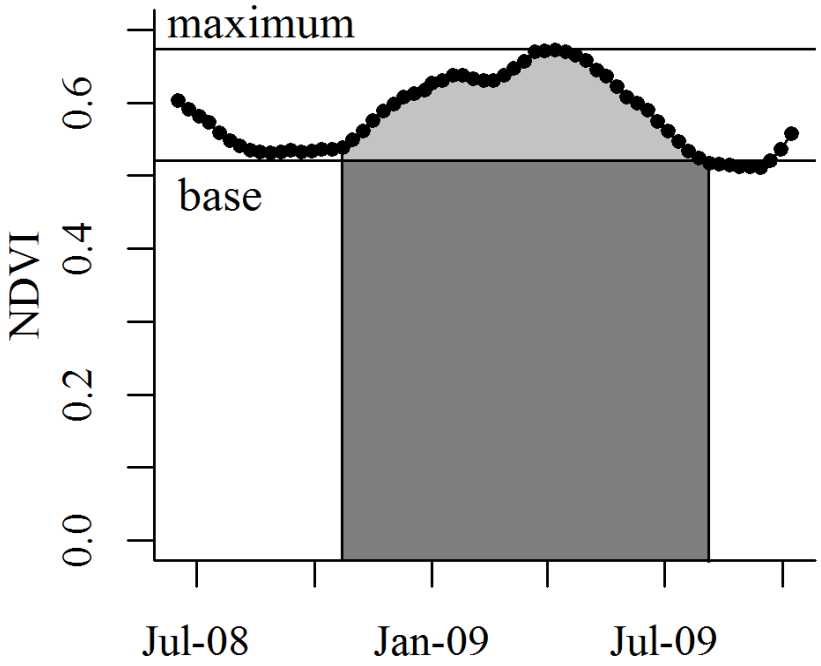

Figure 18: Seasonal growth metrics, illustrated with NDVI data for the 2008 – 2009 growing season. The maximum and base values are indicated with horizontal lines. The amplitude is the difference of these values. The large integral is the total area under the curve (all shaded area) and the small integral is the area between the base value and the growth curve (lighter shaded area).

The maximum value is a useful metric because it is related to the seasonal peak vegetation levels, but in post-fire chaparral, this maximum value might actually represent high NIR reflectance contributions from herbaceous annual vegetation that thrives during the wet winter and spring, but dies back by summer. The base value is likely a better metric to capture the levels of evergreen shrub vegetation, since this metric takes the average of the

values before and after the growth of the herbaceous plants. The amplitude provides a metric of seasonal growth, which might reflect the growth patterns of herbaceous plants, especially in the early years of recovery. The small integral provides a metric of seasonal growth throughout the season relative to the summer/autumn period time period when only evergreen shrubs are present. The large integral is related to total vegetation growth throughout the season (Jonsson and Eklundh 2004). The August value is similar to the base value in that it incorporates only evergreen, rather than herbaceous vegetation. However, this metric varies from the base value in that it does not include the value from the beginning of the season, making it perhaps more sensitive to the actual levels of evergreen shrub vegetation at the end of each season.

5. Data analysis

I conducted a series of bi-variate regressions of the SVI seasonal metrics against stand-level biomass. I exhaustively tested the relationships between the growth metrics (maximum, base value, amplitude, small integral, large integral, mid August value) for each of the SVIs (NDVI, EVI, SAVI, NDWI, NDII6, and VARI) against field measures of biomass determined from growth ring analysis for years 5 – 11 post-fire (n = 7). All statistical analyses were conducted using the R statistical software package.

D. Results

The overall patterns of the time series generated from the six SVIs are similar (Figure 19). All show a sharp decline corresponding to the 2002 wildfire, and a period of rapid recovery in the first few years following the fire. Recovery continues steadily throughout the study period, although the final SVI levels remain lower than pre-fire conditions. The final

year of growth (2012 – 2013 growing season) is somewhat lower than the several previous years, but this is likely due to low precipitation in this year (Uyeda et al. in prep). The SVIs tend to be lower for the northern study area compared to the southern study area (Figure 19). This corresponds with the pattern of slightly lower biomass values observed in the northern study area (Figure 20).

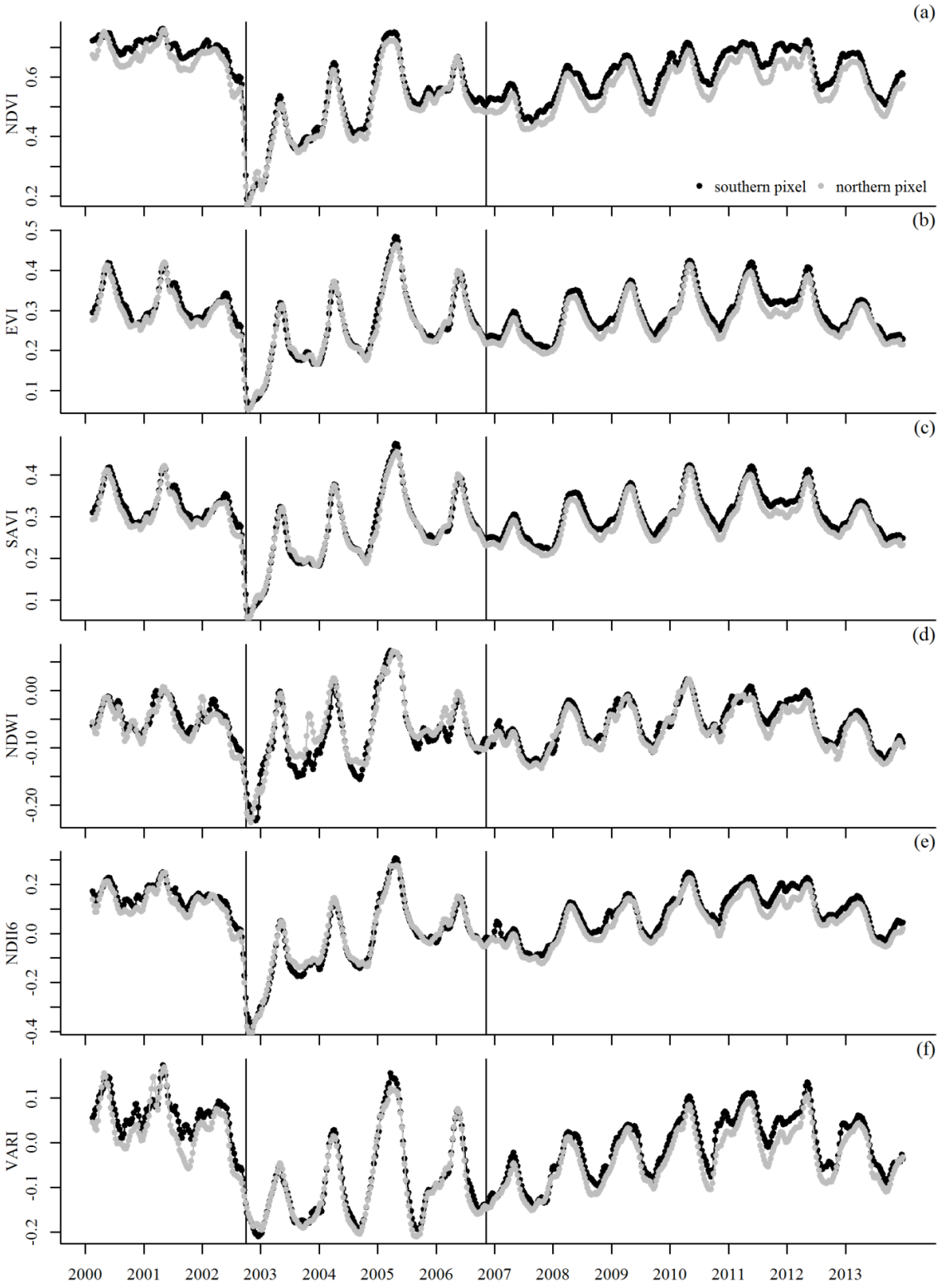

Figure 19: Time series of a) NDVI, b) EVI, c) SAVI d) NDWI, e) NDII6, and f) VARI for northern and southern pixels generated from the MCD43A4 MODIS product. Vertical lines indicate the date of fire (fall 2002) and the start of the field-based biomass time series (fall 2006).

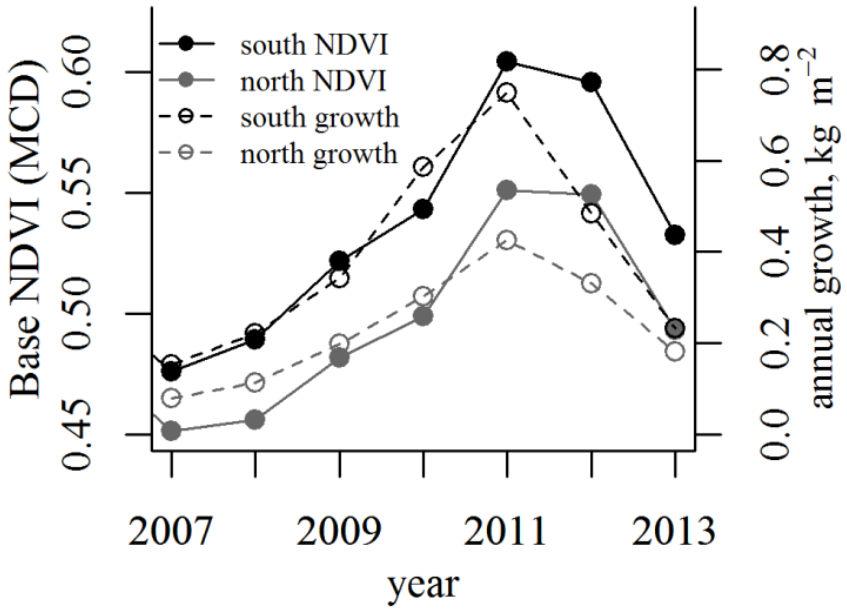

Figure 20: Base NDVI and annual growth for northern and southern study areas

The base value for many of the SVIs tracks closely with annual biomass increment, with coefficient of determination (R^2) values ranging from 0.45 to 0.89 (Figure 21,Table 12, n = 7). The maximum value also shows a close relationship with biomass, with R^2 values ranging from 0.46 to 0.84. The large integral tends to have somewhat lower R^2 values, with a range of 0.28 to 0.92. The small integral is only significant (p <0.01) for one SVI, and amplitude is not significant for any of the SVIs tested. The August values also track closely with annual biomass increment, with R^2 values of 0.56 to 0.89 (Table 13).

In terms of individual SVI comparisons, there are a couple of noteworthy patterns. While most SVIs have significant results (p<0.01) for the base and maximum metrics (particularly in the northern study area), the VARI regressions are significant at the p≤0.05 level for every metric in the northern study area, and nearly every metric in the southern study area.

The SVIs generated from the MCD43A4 MODIS product tend to have somewhat higher R^2 values than the equivalent SVI from the MOD13Q1 MODIS product.

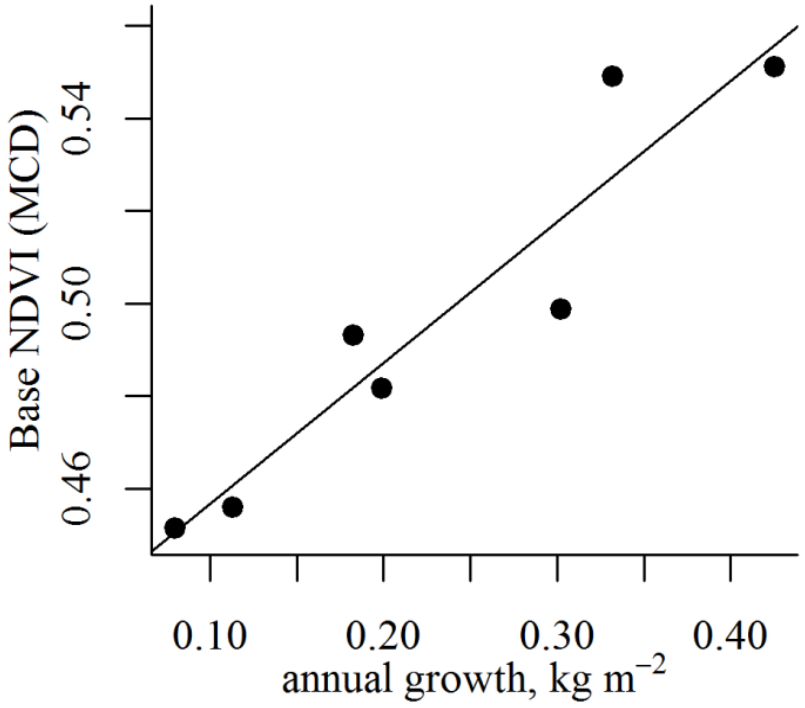

Figure 21: Regression of annual growth and base NDVI for the northern study area. R^2 = 0.89, p = 0.001

Table 12: Regression results for each seasonal metric and annual biomass increment from the two study areas (n = 7). Shading indicates that regression results are significant at p = 0.01.

	northern study area									
	Maximum		Base		Amplitude		Large integral		Small integral	
	R^2	p	R^2	p	R^2	p	R^2	p	R^2	p
NDVI (MOD)	0.57	0.049	0.79	0.008	0.04	0.660	0.46	0.093	0.23	0.273
NDVI (MCD)	0.77	0.009	0.89	0.001	0.12	0.444	0.66	0.027	0.42	0.118
EVI (MOD)	0.57	0.048	0.85	0.003	0.25	0.258	0.6	0.042	0.4	0.130
EVI (MCD)	0.74	0.013	0.86	0.003	0.37	0.150	0.47	0.089	0.2	0.311
SAVI	0.74	0.013	0.86	0.003	0.34	0.170	0.47	0.087	0.2	0.311
NDWI	0.46	0.095	0.82	0.005	0.1	0.480	0.44	0.104	0.33	0.177
NDII6	0.73	0.014	0.77	0.009	0.18	0.340	0.83	0.004	0.36	0.156
VARI	0.83	0.004	0.8	0.007	0.68	0.022	0.9	0.001	0.81	0.006
	southern study area									
	Maximum		Base		Amplitude		Large integral		Small integral	
	R^2	p	R^2	p	R^2	p	R^2	p	R^2	p
NDVI (MOD)	0.64	0.030	0.65	0.029	0.10	0.482	0.42	0.118	0.36	0.155
NDVI (MCD)	0.66	0.027	0.73	0.014	0.00	0.911	0.28	0.218	0.18	0.344
EVI (MOD)	0.65	0.028	0.76	0.010	0.16	0.369	0.59	0.045	0.56	0.052
EVI (MCD)	0.84	0.004	0.68	0.023	0.53	0.064	0.68	0.022	0.29	0.217
SAVI	0.83	0.004	0.68	0.023	0.51	0.070	0.74	0.013	0.34	0.171
NDWI	0.73	0.015	0.87	0.002	0.09	0.504	0.92	0.001	0.22	0.293
NDII6	0.69	0.021	0.45	0.098	0.28	0.224	0.73	0.015	0.43	0.112
VARI	0.68	0.022	0.59	0.044	0.50	0.078	0.70	0.019	0.80	0.007

Spectral Vegetation Indices tested include Normalized Difference Vegetation Index calculated using MOD13Q1 (NDVI (MOD)), and calculated using MCD43A4 (NDVI (MCD)), Enhanced Vegetation Index calculated using MOD13Q1 (EVI (MOD)), and using MCD43A4 (EVI (MCD), Soil Adjusted Vegetation Index (SAVI), Normalized Difference Water Index (NDWI), Normalized Difference Infrared Index 6 (NDII6), and Vegetation Atmospherically Resistant Index (VARI). SAVI, NDWI, NDII6, and VARI were calculated using MCD43A4.

Table 13: Regression results for August SVIs and annual biomass increment from the two study areas (*n* = 7)

	north	
	R^2	*p*
NDVI (MOD)	0.69	0.021
NDVI (MCD)	0.85	0.003
EVI (MOD)	0.56	0.053
EVI (MCD)	0.68	0.022
SAVI	0.70	0.018
NDWI	0.51	0.073
NDII6	0.80	0.006
VARI	0.73	0.014
	south	
	R^2	*p*
NDVI (MOD)	0.64	0.031
NDVI (MCD)	0.84	0.004
EVI (MOD)	0.78	0.009
EVI (MCD)	0.83	0.004
SAVI	0.84	0.003
NDWI	0.81	0.006
NDII6	0.89	0.001
VARI	0.73	0.014

Spectral Vegetation Indices tested include Normalized Difference Vegetation Index calculated using MOD13Q1 (NDVI (MOD)), and calculated using MCD43A4 (NDVI (MCD)), Enhanced Vegetation Index calculated using MOD13Q1 (EVI (MOD)), and using MCD43A4 (EVI (MCD), Soil Adjusted Vegetation Index (SAVI), Normalized Difference Water Index (NDWI), Normalized Difference Infrared Index 6 (NDII6), and Vegetation Atmospherically Resistant Index (VARI). SAVI, NDWI, NDII6, and VARI were calculated using MCD43A4.

E. Discussion

In this study, I explored the relationship between ground-based measurements of annual chaparral growth and MODIS-based seasonal growth metrics for the fourth through eleventh year following burning by a wildfire. I found that up to 92% of the variance in MODIS growth metrics can be explained by annual biomass growth. This strong relationship indicates that this integrated field-satellite measurement and scaling approach is sufficiently

promising to further develop and implement for mapping chaparral (and likely other shrubland) biomass growth at regional scales.

The variation in SVI values throughout the growing season track with seasonal patterns of live fuel moisture (LFM), which is related to the timing and quantity of annual precipitation (Dennison et al. 2008). The SVIs examined in this study are well known to track with LFM , particularly during the annual "dry down" period during the summer drought (Peterson et al. 2008). In particular, VARI has been shown to have a close relationship with field-measured LFM (Stow et al. 2005).

While the base value closely co-varies with biomass for many of the SVIs examined, the August SVIs showed similar close relationships. This is noteworthy because the data processing requirements for single date per year SVIs are much reduced when compared with the full temporal resolution of 46 images per year (for the 8 day MODIS products). It is not surprising that amplitude and small integral values are not closely related to annual biomass growth, as these metrics are more closely related to the herbaceous vegetation component. I expected the large integral to be more closely related to shrub growth, as this metric is related to total productivity. However, it is possible that the herbaceous component still present at this phase of recovery contributed to SVIs summed to calculate the large integral, resulting in a pattern distinct from that of shrub recovery. While shrubs recover quickly in the years following a fire, herbaceous cover can remain relatively high in the early post-fire years (Keeley et al. 2005), possibly contributing to the total productivity signal of MODIS SVI trajectories.

While the results of this study indicate that base value and August value are closely related to annual growth for nearly all the SVIs examined, it is more difficult to identify the most promising SVI based on only two study areas (and two associated MODIS pixels). The SVI with the highest R^2 value for a given seasonal metric in the northern study area is not necessarily the SVI with the highest value in the southern area. It would be necessary to extend the study over larger areas in order to determine the optimal SVI, which would require substantial field personnel resources and effort.

Another area for further research is to determine how the relationship between SVIs and biomass changes as stands reach maturity. Based on the growth trajectories measured in previous studies, biomass values measured at 11-years-old are likely to at least double over the next decade of post-fire recovery (Riggan et al. 1988; Uyeda et al. in prep). The rate of biomass accumulation typically declines with time within the first two decades of recovery, but there appears to be positive net accumulation at least until an age of approximately 40 years (Black 1987; Rundel and Parsons 1979). NDVI in particular is prone to saturate at high biomass values (Huete et al. 2002). As the rate of biomass accumulation declines and SVIs become more likely to saturate in mature stands, the overall relationship is likely to change.

Patterns of biomass growth are important for understanding issues such as ecosystem health and fuel loading. Chaparral subject to frequent fires is prone to type conversion, resulting in sub-shrubs or grasses in areas once dominated by dense shrubs (Lippitt et al. 2012). Climate change is also likely to change patterns of productivity. Results of field (Prieto et al. 2009) and modeling (Tague et al. 2009) studies suggest that productivity in Mediterranean-type climate shrublands could be reduced in a warmer climate as greater

water stress is placed on plants. However, a warmer climate combined with greater concentrations of CO_2 could actually increase chaparral productivity (Tague et al. 2009). It is not yet clear how these potential changes in productivity will change fuel accumulation and ultimately, fire patterns. This study shows that there is strong potential for using the combination of remotely sensed imagery and shrub growth rings to measure annual changes in biomass accurately across large spatial scales, which could be used to monitor ecosystem recovery and change through time.

Chapter 5: Conclusion

A. Summary and synthesis

The overall goal of this study is to develop, test and implement procedures for tracking short- and long-term changes in biomass accumulation in southern California chaparral, and to understand spatial and temporal patterns of productivity and fuel accumulation. I accomplish this goal by extending the results of detailed field work across larger spatial extents using remote sensing methods. In chapter 2, I examine differences in biomass and species composition in adjacent 7-, 28-, and 68-year-old stands of chaparral. I find that shrub biomass within the study area remains high in chaparral that is at least 68-years-old. In all age classes, I find a wide range of biomass values, indicating a high degree of spatial variability within chaparral. *Adenostoma fasciculatum* is dominant in the youngest stand, and *Quercus berberidifolia* is dominant in the two older stands, although it is not clear whether this difference is due to site differences or an age-related shift in dominance.

In Chapter 3, I estimate biomass accumulation at an annual scale from 4- to 11-years post-fire using measurements taken from shrub growth rings. This approach is a promising technique for estimating several years of post-fire growth using a single season of field work. I also examine environmental factors related to temporal variation in growth (precipitation) and spatial variation in growth (solar irradiation and flow accumulation). While annual growth closely tracks patterns of annual precipitation, solar irradiation and flow accumulation were not found to be significant covariates with total biomass

In Chapter 4, I test the relationship between the annual growth measurements estimated in Chapter 3 with satellite-based seasonal growth metrics to determine the potential for

extending estimation of annual growth patterns across larger spatial extents. I find a strong relationship between annual biomass estimated from annual growth rings and satellite-based seasonal growth metrics. While additional research would be required prior to utilizing these relationships over larger spatial extents, this integrated field-satellite measurement and scaling approach is sufficiently promising to further develop and implement for mapping chaparral biomass growth at regional scales.

Field work in chaparral is arduous and slow due to dense biomass and often steep terrain. Spatial scales relevant in fire ecology are typically vastly greater than is feasible to study using field work alone. In addition, biomass accumulation occurs over a period of decades, making it difficult to adequately characterize patterns in a single year of field work. In this research, I use high spatial resolution and lower temporal resolution airborne imagery and coarse spatial resolution and high temporal resolution satellite imagery to extend estimates of biomass across space and through time. Many of the existing field-based studies of biomass accumulation in chaparral took place in the 1980s (Black 1987; Gray 1982; Riggan et al. 1988; Schlesinger and Gill 1980). My research provides a valuable update to these studies, and extends the results of field work with remote sensing data not available in that time period. The method I develop for relating shrub growth rings to satellite-based seasonal growth metrics has the potential to greatly improve the temporal and spatial resolution of biomass accumulation estimates.

An increased understanding of patterns of biomass accumulation could improve the accuracy of fuel mapping, which is important to fire management. Fuel maps are used for many purposes before and during wildfires, including planning fuel reduction treatments and modeling fire behavior (Keane et al. 2001). Fuel treatments can have significant ecological

costs, including the establishment of non-native vegetation, but more strategic placement of fuel breaks could help reduce these impacts (Merriam et al. 2006; Syphard et al. 2011). Fire behavior modeling relies on coarse-scale fuel models that do not take into account biomass accumulation through time or the wide range in biomass often present within a single stand (Riggan et al. 2010). Understanding biomass accumulation over a wide range of temporal and spatial scales could help to improve the inputs to fire behavior models, increasing the accuracy of the predicted behavior.

B. Future directions

One extension of this work would be to test the relationship between the field measurements of annual growth and satellite-based growth metrics over larger spatial extents and for longer time periods. I conducted extensive field sampling in this exploratory study, so an important first step would be to use the existing field data to determine the minimum number of field plots necessary to adequately characterize annual change in a given MODIS ground resolution element. Reducing the number of field plots required would allow finite resources to stretch further, allowing for the largest study area possible.

It would also be useful to test SVIs derived from the Landsat surface reflectance product for biomass tracking at fine spatial resolutions. A key advantage of utilizing MODIS products for this analysis is the high temporal resolution, which allows the calculation of metrics of growth based on information from the entire growing season. However, the preliminary results indicate that data from a single summer date might be sufficient to characterize annual growth. This suggests that Landsat data could be used, which are available at a coarser but adequate temporal resolution, and a finer spatial resolution compared to MODIS data.

Another follow-up component would be to conduct a multi-year accuracy assessment of the growth ring method for predicting biomass by comparing the increase in biomass estimated by repeatedly measuring stem diameters. This would require establishing new field plots and measuring all stems to estimate biomass in year one, as well as harvesting shrubs outside of the plot area to calculate the species-specific regression equations of stem basal area and biomass. After at least one year has elapsed, it would be necessary to repeat all stem measurements to estimate the plot level biomass increment. At that time, stem cross-sections could also be collected from some (or possibly all) of the shrubs to estimate the increase in biomass over the one year period, and the harvested shrubs could also be weighed to calculate a new regression equation of stem basal area and biomass. Repeating this process over a sufficiently large number of field plots would be very labor-intensive, and was not possible in the limited time period of my dissertation research. A related factor would be to determine the extent to which growth rates measured in obligate-seeding species provide a reasonable metric of growth in resprouting species.

Further study of the relationship between biomass and factors related to terrain (solar irradiation and flow accumulation) would also be helpful to determine if these factors are important at larger spatial scales or in older stands of chaparral. This analysis would help to explain the spatial variation in chaparral growth, which could improve the accuracy of regional estimates of biomass accumulation.

In addition, it could be useful to further explore of the use of shrub height data for estimating shrub biomass. I recorded the approximate height of every shrub measured during plot sampling at both field sites, so I have an extensive record of the relationship between estimated biomass and shrub height. While my preliminary investigation revealed that

individual shrubs with widely varying biomass levels are approximately the same height in a given stand, measurements of shrub height could provide a quick estimate of biomass variation across different stands. This approach could be helpful in situations where the labor-intensive process of measuring the stem diameters of individual shrubs is not practical.

References

Abràmoff MD, Magalhães PJ, Ram SJ (2004) Image Processing with ImageJ. Biophotonics Int 11:36–42.

Baeza MJ, Santana VM, Pausas JG, Vallejo VR (2011) Successional trends in standing dead biomass in Mediterranean basin species. J Veg Sci 22:1–8.

Baskerville G (1972) Use of logarithmic regression in the estimation of plant biomass. Can J For Res 2:49–53.

Black CH (1987) Biomass, nitrogen, and phosphorus accumulation over a southern California fire cycle chronosequence. In: Tenhunen JD, Catarino FM, Lange OL, Oechel WC (eds) Plant Response to Stress - Funct. Anal. Mediterr. Ecosyst. Springer, pp 445 – 458

Bouriaud O, Bréda N, Dupouey JL, Granier A (2005) Is ring width a reliable proxy for stem-biomass increment? A case study in European beech. Can J For Res 35:2920–2933.

Breshears DD, Allen CD (2002) The importance of rapid, disturbance-induced losses in carbon management and sequestration. Glob Ecol Biogeogr 11:1–5.

Burgan R, Rothermel RC (1984) BEHAVE: fire behavior prediction and fuel modeling system--FUEL subsystem.

Bush R, Brand G (2008) Lake States (LS) Variant Overview - Forest Vegetation Simulator. Internal Report. Fort Collins, CO

Clark DA, Brown S, Kicklighter DW, et al. (2001) Measuring net primary production in forests: concepts and field methods. Ecol Appl 11:356–370.

Coale T, Deveny A, Fox L (2011) Growth, fire history, and browsing recorded in wood rings of shrubs in a mild temperate climate. Ecology 92:1020–1026.

Countryman CM, Dean WA (1979) Measuring moisture content in living chaparral: a field user's manual. Berkeley, CA, Gen. Tech. Rep. PSW-36. USDA Forest Service. Pacific Southwest Forest and Range Experiment Station

Countryman CM, Philpot CW (1970) Physical characteristics of chamise as a wildland fuel. Res Pap PSW- 66, Pacific Southwest For Range Exp Station For Serv US Dep Agric Berkeley, CA 16.

Dahlin KM, Asner GP, Field CB (2012) Environmental filtering and land-use history drive patterns in biomass accumulation in a mediterranean-type landscape. Ecol Appl 22:104–18.

Daly C, Halbleib M, Smith JI, et al. (2008) Physiographically sensitive mapping of climatological temperature and precipitation across the conterminous United States. Int J Climatol 28:2031–2064.

Davis S, Ewers F, Sperry J, et al. (2002) Shoot dieback during prolonged drought in Ceanothus (Rhamnaceae) chaparral of California: a possible case of hydraulic failure. Am J Bot 89:820 – 828.

Davis S, Mooney H (1986) Water use patterns of four co-occurring chaparral shrubs. Oecologia 70:172–177.

Dennison PE, Moritz MA, Taylor RS (2008) Evaluating predictive models of critical live fuel moisture in the Santa Monica Mountains , California. Int J Wildl Fire 17:18–27.

Dougherty R, Riggan PJ (1982) Operational Use of Prescribed Fire in Southern California Chaparral. Proc. Symp. Dyn. Manag. Mediterr. Ecosyst.

Dunn PH, Barro SC, Wells II WG, et al. (1988) The San Dimas experimental forest: 50 years of research. Gen Tech Rep PSW-104, USDA For Serv Pacific Southwest For Range Exp Stn 54.

Duren OC, Muir PS (2010) Does fuels management accomplish restoration in southwest Oregon, USA, chaparral? Insights from age structure. Fire Ecol 6:76–96.

Easterling DR, Meehl G a, Parmesan C, et al. (2000) Climate extremes: observations, modeling, and impacts. Science 289:2068–74.

Fritts HC, Swetnam TW (1989) Dendroecology: A Tool for Evaluating Variations in Past and Present Forest Environments. Adv Ecol Res 19:111–188.

Gao BC (1996) NDWI - A normalized difference water index for remote sensing of vegetation liquid water from space. Remote Sens Environ 58:257–266.

Garbulsky M, Peñuelas J, Ogaya R, Filella I (2013) Leaf and stand-level carbon uptake of a Mediterranean forest estimated using the satellite-derived reflectance indices EVI and PRI. Int J Remote Sens 34:1282 – 1296.

Gitelson AA, Kaufman YJ, Stark R, Rundquist D (2002) Novel algorithms for remote estimation of vegetation fraction. Remote Sens Environ 80:76 – 87.

Gray JT (1982) Community structure and productivity in Ceanothus chaparral and coastal sage scrub of southern California. Ecol Monogr 52:415–435.

Green LR (1970) An experimental prescribed burn to reduce fuel hazard in chaparral. USDA For Serv Res Note PSW-216, Berkeley, CA 6.

Hanes TL (1971) Succession after Fire in the Chaparral of Southern California. Ecol Monogr 41:27–52.

Henry MC, Hope AS (1998) Monitoring post-burn recovery of chaparral vegetation in southern California using multi-temporal satellite data. Int J Remote Sens 19:3097–3107.

Hiers JK, O'Brien JJ, Mitchell RJ, et al. (2009) The wildland fuel cell concept: an approach to characterize fine-scale variation in fuels and fire in frequently burned longleaf pine forests. Int J Wildl Fire 18:315.

Hope AS, Tague C, Clark R (2007) Characterizing post-fire vegetation recovery of California chaparral using TM/ETM+ time-series data. Int J Remote Sens 28:1339–1354.

Huete a. R (1988) A Soil-Adjusted Vegetation Index (SAVI). Remote Sens Environ 309:295–309.

Huete A, Didan K, Miura T, et al. (2002) Overview of the radiometric and biophysical performance of the MODIS vegetation indices. Remote Sens Environ 83:195–213.

Hunt ERJ, Rock BN (1989) Detection of changes in leaf water content using Near- and Middle-Infrared reflectances. Remote Sens Environ 30:43–54.

Jonsson P, Eklundh L (2004) TIMESAT- a program for analyzing time-series of satellite sensor data. Comput Geosci 30:833–845.

Kaye JP, Romanyà J, Vallejo VR (2010) Plant and soil carbon accumulation following fire in Mediterranean woodlands in Spain. Oecologia 164:533–43.

Keane RE, Agee JK, Fulé P, et al. (2008) Ecological effects of large fires on US landscapes : benefit or catastrophe ? Int J Wildl Fire 17:696.

Keane RE, Burgan R, van Wagtendonk J (2001) Mapping wildland fuels for fire management across multiple scales: Integrating remote sensing, GIS, and biophysical modeling. Int J Wildl Fire 10:301–319.

Keeley J (2000) Chaparral. In: Barbour M, Billings W (eds) North Am. Terr. Veg., 2nd editio. Cambridge University Press, pp 203 – 253

Keeley JE (1992) Demographic structure of California chaparral in the long-term absence of fire. J Veg Sci 3:79–90.

Keeley JE (1993) Utility of growth rings in the age determination of chaparral shrubs. Madrono 40:1–14.

Keeley JE, Fotheringham CJ, Baer-Keeley M (2005) Determinants of postfire recovery and succession in mediterranean-climate shrublands of California. Ecol Appl 15:1515–1534.

Keeley JE, Fotheringham CJ, Moritz MA (2004) Lessons from the October 2003 Wildfires in Southern California. J. For. 102:

Keeley JE, Keeley SC (1981) Post-Fire Regeneration of Southern California Chaparral. Am J Bot 68:524.

Keeley JE, Safford H, Fotheringham CJ, et al. (2009) The 2007 southern California wildfires: lessons in complexity. J. For.

Keeley JE, Zedler PH (2009) Large, high-intensity fire events in southern California shrublands: debunking the fine-grain age patch model. Ecol Appl 19:69–94.

Keeley SC, Keeley JE, Hutchinson S, Johnson A (1981) Postfire succession of the herbaceous flora in southern California chaparral. Ecology 62:1608–1621.

Kinoshita AM, Hogue TS (2011) Spatial and temporal controls on post-fire hydrologic recovery in Southern California watersheds. Catena 87:240–252.

Van Leeuwen WJD, Casady GM, Neary DG, et al. (2010) Monitoring post-wildfire vegetation response with remotely sensed time-series data in Spain, USA and Israel. Int J Wildl Fire 19:75.

Lippitt CL, Stow DA, O'Leary JF, Franklin J (2012) Influence of short-interval fire occurrence on post-fire recovery of fire prone shrublands in California , USA. Int J Wildl Fire 22:184–193.

Lu D (2006) The potential and challenge of remote sensing based biomass estimation. Int J Remote Sens 27:1297–1328.

Mahall BE, Wilson CS (1986) Environmental Induction and Physiological Consequences of Natural Pruning in the Chaparral Shrub Ceanothus megacarpus. Bot Gaz 147:102–109.

Malmström C, Thompson M, Juday GP, et al. (1997) Interannual variation in global-scale net primary production: Testing model estimates. Global Biogeochem Cycles 11:367 – 392.

McMichael CE, Hope AS, Roberts DA, Anaya MR (2004) Post-fire recovery of leaf area index in California chaparral: a remote sensing-chronosequence approach. Int J Remote Sens 25:4743–4760.

Merriam KE, Keeley JE, Beyers JL (2006) Fuel breaks affect nonnative species abundance in Californian plant communities. Ecol Appl 16:515–527.

Moritz MA, Keeley JE, Johnson EA, Schaffner AA (2004) Testing a Basic Assumption of Shrubland Fire Management : How Important Is Fuel Age ? Front Ecol Environ 2:67–72.

Pasquini SC, Vourlitis GL (2010) Post-fire primary production and plant community dynamics in chaparral stands exposed to varying levels of nitrogen deposition. J Arid Environ 74:310–314.

Paysen TE, Cohen JD (1990) Chamise chaparral dead fuel fraction is not reliably predicted by age. West J Appl For 5:127–131.

Peterson SH, Roberts DA, Dennison PE (2008) Mapping live fuel moistures with MODIS data: A multiple regression approach. Remote Sens Environ 112:4272 – 4284.

Peterson SH, Stow DA (2003) Using multiple image endmember spectral mixture analysis to study chaparral regrowth in southern California. Int J Remote Sens 24:4481–4504.

Prieto P, Peñuelas J, Llusià J, et al. (2009) Effects of experimental warming and drought on biomass accumulation in a Mediterranean shrubland. Plant Ecol 205:179–191.

Regelbrugge JC, Conard SG (1996) Biomass and fuel characteristics of chaparral in southern California. 13th Conf. Fire For. Meteorol.

Riaño D, Chuvieco E, Salas J, et al. (2002a) Generation of fuel type maps from Landsat TM images and ancillary data in Mediterranean ecosystems. Can J For Res 32:1301–1315.

Riaño D, Chuvieco E, Ustin S, et al. (2002b) Assessment of vegetation regeneration after fire through multitemporal analysis of AVIRIS images in the Santa Monica Mountains. Remote Sens Environ 79:60–71.

Rich P, Dubayah RC, Hetrick W, Saving S (1994) Using Viewshed Models to Calculate Intercepted Solar Radiation: Applications in Ecology. Am Soc Photogramm Remote Sens Tech Pap 524–529.

Riggan PJ, Franklin S, Brass J, Brooks F (1994) Perspectives on fire management in Mediterranean ecosystems of southern California. In: Moreno JM, Oechel WC (eds) role fire Mediterr. Ecosyst. Springer-Verlag, New York, pp 140–162

Riggan PJ, Goode S, Jacks PM, Lockwood RN (1988) Interaction of Fire and Community Development in Chaparral of Southern California. Ecol Monogr 58:156–176.

Riggan PJ, Wolden LG, Tissell RG, et al. (2010) Remote Sensing Fire and Fuels in Southern California. Proc. 3rd Fire Behav. Fuels Conf. Oct. 25-29, 2010, Spokane, Washington,

USA. International Association of Wildland Fire, Birmingham, Alabama, USA, pp 1–14

Roberts DA, Peterson SH, Sweeney P., Rechel J (2006) Evaluation of AVIRIS and MODIS measures of live fuel moisture and fuel condition in a shrubland ecosystem in southern California. J Geophys Res - Biogeosciences 111:1–48.

Roder A, Hill J, Duguy B, et al. (2008) Using long time series of Landsat data to monitor fire events and post-fire dynamics and identify driving factors. A case study in the Ayora region (eastern Spain). Remote Sens Environ 112:259–273.

Rouse JW, Haas RH, Schell JA, Deering DW (1973) Monitoring vegetation systems in the Great Plains with ERTS. Third ERTS Symp NASA SP-351 I 309–317.

Rundel PW, Parsons DJ (1979) Structural Changes in Chamise (Adenostoma fasciculatum) along a Fire-Induced Age Gradient. J Range Manag 32:462–466.

Saruwatari W, Davis SD (1989) Tissue water relations of three chaparral shrubs species after wildfire. Oecologia 80:303–308.

Schlesinger WH, Gill DS (1980) Biomass, production, and changes in the availability of light, water, and nutrients during the development of pure stands of the chaparral shrub, Ceanothus megacarpus, after fire. Ecology 61:781–789.

Schlesinger WH, Gray JT, Gill DS, Mahall BE (1982) Ceanothus megacarpus chaparral: a synthesis of ecosystem processes during development and annual growth. Bot Rev 48:71–117.

Schwilk DW (2003) Flammability is a Niche Construction Trait : Canopy Architecture Affects Fire Intensity. Am Nat 162:725–733.

Specht R (1969) A comparison of the sclerophyllous vegetation characteristic of mediterranean type climates in France, California, and southern Australia. II. Dry matter, energy, and nutrient accumulation. Aust J Bot 17:293–308.

Sprugel D (1983) Correcting for bias in log-transformed allometric equations. Ecology 64:209–210.

Stohlgren T, Parsons DJ, Rundel PW (1984) Population structure of Adenostoma fasciculatum in mature stands of chamise chaparral in the southern Sierra Nevada, California. Oecologia 64:87–91.

Stow D, Hamada Y, Coulter L, Anguelova Z (2008) Monitoring shrubland habitat changes through object-based change identification with airborne multispectral imagery. Remote Sens Environ 112:1051–1061.

Stow DA, Niphadkar M, Kaiser J (2005) MODIS-derived visible atmospherically resistant index for monitoring chaparral moisture content. Int J Remote Sens 26:3867–3873.

Syphard AD, Keeley JE, Brennan TJ (2011) Comparing the role of fuel breaks across southern California national forests. For Ecol Manage 261:2038–2048.

Tague C, Seaby L, Hope AS (2009) Modeling the eco-hydrologic response of a Mediterranean type ecosystem to the combined impacts of projected climate change and altered fire frequencies. Clim Change 93:137–155.

Uyeda KA, Stow DA, O'Leary JF, et al. Spatial variation of fuel loading within varying aged stands of chaparral (in review). Appl. Veg. Sci.

Uyeda KA, Stow DA, O'Leary JF, et al. Chaparral growth ring analysis as an indicator of stand biomass development. (in prep)

Uyeda KA, Stow DA, Riggan PJ (2015) Tracking MODIS NDVI time series to estimate fuel accumulation. Remote Sens Lett 6:587–596.

Wang J, Rich PM, Price KP, Kettle WD (2004) Relations between NDVI and tree productivity in the central Great Plains. Int J Remote Sens 25:3127–3138.

Weise DR, Zhou X, Sun L, Mahalingam S (2005) Fire spread in chaparral —" go or no-go ?" Int J Wildl Fire 14:99–106.

Yool S, Eckhardt D, Estes J, Cosentino M (1985) Describing the Brushfire Hazard in Southern California. Ann Assoc Am Geogr 75:417–430.

Zammit C, Zedler P (1993) Size structure and seed production in even-aged populations of Ceanothus greggii in mixed chaparral. J Ecol 81:499–511.